Late Holocene cryptotephra and a provisional 15,000-year Bayesian age model for Cascade Lake, Alaska

Lauren J. Davies[1,2], Britta J. L. Jensen[1], Darrell S. Kaufman[3]

[1]Department of Earth and Atmospheric Sciences, University of Alberta, Edmonton, AB, Canada
[2]Department of Geography, University of Cambridge, Cambridge, UK
[3]School of Earth and Sustainability, Northern Arizona University, Flagstaff, Arizona, USA

Correspondence to: Lauren J. Davies (ld636@cam.ac.uk)

Abstract. Multiple chronometers can be employed for dating Holocene palaeoenvironmental records, each with its own inherent strengths and weaknesses. Radiocarbon dating is one of the most widely used techniques for producing chronologies, but its application at high-latitude sites can sometimes be problematic. Here, cryptotephra identified in a core from Cascade Lake, Arctic Alaska, highlight and help to resolve an old bias in Late Holocene radiocarbon dates in the top 1.42 m of the sediment sequence. Identifiable geochemical populations of cryptotephra are shown to be present in detectable concentrations in sediment from the north flank of the Brooks Range for the first time. Major element glass geochemical correlations are demonstrated between ultra-distal cryptotephra and reference samples from the Late Holocene caldera forming eruption of Opala, Kamchatka, as well as three eruptions in North America: the White River Ash (northern lobe), Ruppert tephra and the Late Holocene caldera forming eruption of Aniakchak. The correlated ages of these cryptotephra provide evidence for an old-carbon effect and support preliminary PSV ages reported for Cascade Lake. Chronological data from Cascade Lake were then combined using a Bayesian approach to generate an age-depth model that extends back through the Late Holocene, and provisionally to 15,000 cal yr BP.

1 Introduction

The accuracy and precision of ages and chronological models produced from sedimentary records directly impacts the utility and value of the associated proxies used for palaeoenvironmental reconstructions. In Arctic North America, the majority of Holocene to late Pleistocene palaeoenvironmental reconstructions are produced from lake and peat deposits (e.g. Kaufman et al., 2016), and often rely on radiocarbon (^{14}C) dating to develop age models.

However, there are several issues that can affect the application and interpretation of ^{14}C ages in Arctic regions. Firstly, there may be a lack of organic material in lake sediment cores, or the terrestrial macrofossils that are often preferred for dating (e.g. Oswald et al., 2005; Turney et al., 2000) may be absent. This can be a particular problem for sediments that accumulated during colder periods. Secondly, high-latitude regions often have an abundance of old carbon due to slow rates of decomposition in cold, typically nutrient poor soils (e.g.

Deleted: from Cascade Lake, Alaska: supporting data for
Deleted: 21
Deleted: multi-chronometer
Deleted: the Late Holocene portion of
Deleted: a divergence identified between
Deleted: and paleomagnetic secular variation (PSV) data
Deleted: 5
Deleted: support the PSV ages reported in Steen et al. (this volume) and …
Deleted: in
Deleted: the
Deleted: to 21

Gaglioti et al., 2014; Schuur et al., 2008), erosion from the surrounding sediments or bedrock, and the reworking and redeposition of older, well-preserved macrofossils (e.g. Kennedy et al., 2010).

More broadly, ^{14}C samples can also be affected by issues relating to sample selection, remobilisation, the hard-water effect and contamination (for a general review of these topics see Olsson, 1974; Lowe and Walker, 2000). These factors can contribute to complicated age models for Arctic sediments that require careful independent verification. For example, the use of bulk sediments for dating has been shown to incorporate organic fractions of varying ages (e.g. Brock et al., 2011; Nelson et al., 1988) and hard-water effects have long been known in North American lakes (e.g. Abbott and Stafford, 1996; Karrow and Anderson, 1975; Moore et al., 1998). It is important to recognise that not all ^{14}C ages are affected by these issues, but at Arctic sites their accuracy and reliability cannot be assumed. Additional validation and reassurance provided, for example, by published details of the dated material and the stratigraphic sequences they were extracted from, overlapping independent chronological data, replicate dates, etc, is therefore valuable when attributing confidence to resultant age models.

The combination of multiple chronometers has been successfully used to highlight differences between chronological methods and produce more accurate final age models for lacustrine and peat cores (Davies et al., 2018; Tylmann et al., 2016). Two additional techniques that have been applied in Arctic areas are discussed here - palaeomagnetic secular variation (PSV) and tephrochronology.

1.1 Palaeomagnetic chronologies

In recent years there have been an increasing number of studies looking to improve chronologies of late Quaternary Arctic sedimentary sequences by using palaeomagnetic data (e.g. Barletta et al., 2008; Deschamps et al., 2018; Lund et al., 2016; Ólafsdóttir et al., 2013). Sediment records can be sensitive to palaeomagnetic secular variation (PSV) – small directional changes in the geomagnetic field (Cox, 1970) that are preserved in sediment through the alignment of magnetic mineral grains with Earth's ambient field around the time of deposition. Tie-points, identified using peaks and troughs, can then be dated and used as correlative chronostratigraphic tools. These ages can be produced from both individual site measurements and geomagnetic model predictions. PSV correlation techniques are useful as they can produce more frequent data points and be applied beyond the limits of ^{14}C dating, or

Deleted: , e.g.
Deleted: resulting
Deleted: Sediments at high-latitude sites
Deleted: calculations

where organic material is not preserved. Their use, however, is limited geographically as high-latitude geomagnetic field dynamics are spatially complex (e.g. Stoner et al., 2013).

Steen (2016) reports preliminary PSV-correlated ages for cores from Cascade Lake, Alaska, that have substantial offsets during the Late Holocene from ^{14}C ages from the same sediment. In the upper sections of the core sequence, ^{14}C ages are up to ~2000 years older than palaeomagnetic correlated ages. When using multiple chronometers from the same sediment there is not always coherence or clear agreement between the results, as seen here, and additional chronological information is required to produce a reliable age-model. In this study, tephrochronology was applied to Cascade Lake sediments to investigate this chronological offset.

Deleted: Steen et al. (this volume) report

Deleted: Over

Deleted: top 175 cm

Deleted: ,

Deleted: . Here,

Deleted: third chronostratigraphic technique –

Deleted: –

Deleted: resolve the

1.2 Cryptotephra chronologies

Cryptotephra - non-visible horizons of volcanic ash from distal sources - have been studied globally (see, e.g., Davies, 2015; Lowe et al., 2017) and are a useful chronostratigraphic tool (Pilcher et al., 1995; Plunkett, 2006; Swindles et al., 2010). Where correlations can be made with well-dated tephra (e.g. historical eruptions, or tephra preserved within annually resolved records), tightly constrained associated ages can be included in age-depth models (e.g. Schoning et al., 2005). They can also be used as an independent test of other chronological methods applied to the same record (e.g. Davies et al., 2018; Oldfield et al., 1997).

Deleted: –

Deleted: .

In Alaska and northern Canada the majority of tephra studies have been limited to areas where visible tephra are present and only a few studies have discussed cryptotephra (de Fontaine et al., 2007; Lakeman et al., 2008; Monteath et al., 2017; Payne et al., 2008; Zoltai, 1989). However, there is significant potential for cryptotephra to be found in Alaska as it is downwind of a large number of volcanoes known to have been active over the Holocene (Fig. 1; Alaska Volcano Observatory, 2016; Global Volcanism Program, 2013). Of Alaska's 130 volcanoes and volcanic fields, 96 have been active either historically or within the Holocene (Miller et al., 1998) and historical observations show that 54 volcanoes have been active since ~ 1700 AD alone (Cameron et al., 2020). Here, key tephra are from historical eruptions, or eruptions that produced regionally widespread tephra within Alaska and have precise age estimates (Davies et al., 2016).

Deleted: identified

Deleted: (e.g.

Deleted: .

Deleted: (Miller et al., 1998) and historical observations show that more than 50 volcanoes have been active since ~ 1760 AD alone (Alaska Volcano Observatory, 2016).…

While there are currently no published occurrences of Kamchatkan tephra within Alaska, the large number of Kamchatkan-Kurile volcanoes active in the Holocene can also be considered as a potential source of distal cryptotephra, given prevailing wind directions and

the large number of recorded major explosive eruptions (e.g. Braitseva et al., 1997; Kyle et al., 2011; Ponomareva et al., 2017). Transcontinental distribution of tephra from non-super eruptions has been established (e.g. Cook et al., 2018; Jensen et al., 2014), and Kamchatkan-sourced tephra have been traced to Greenland, Svalbard and the east coast of North America (van der Bilt et al., 2017; Cook et al., 2018; Jensen et al., 2021; Mackay et al., 2016).

Here, ages from Cascade Lake for cryptotephra and radiocarbon techniques were visually compared and then modelled using Bayesian statistical methods to produce a composite age-depth model. Bayesian techniques have been utilised in a wide range of fields to produce detailed age-depth models based on a relatively small number of dates (e.g. Christen et al., 1995; Litton and Buck, 1995) and, through their inclusion of additional (prior) information, they provide more precise interpolations than using raw dates alone (e.g. Blaauw and Christen, 2005; Bronk Ramsey, 2008).

Deleted: , Jensen et al., submitted

Field Code Changed

Deleted: three different chronostratigraphic

Deleted: statistics

Deleted: statistical

2 Materials and Methods

Cascade Lake (68°22'48" N, 154°38'00" W; 990 m asl) lies on the north-central slope of the Brooks Range, the northernmost mountain range in Alaska (Fig. 1). Overall, the Brooks Range is located almost entirely above the Arctic Circle and represents a significant topographic barrier that divides the climatic influences of the Arctic and Pacific Oceans. The lake has an area of ~ 1 km^2 and a maximum depth of ~ 40 m in the main northwestern basin (Fig. 1b) with a total catchment size of ~10 km^2. It presently has no significant inflow and one small outflow, west to Kurupa Lake (~ 920 m asl).

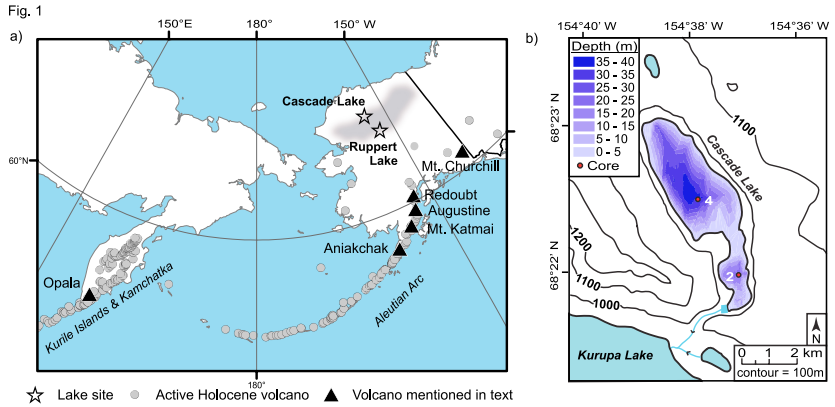

Figure 1: Location map showing Cascade Lake, coring sites, and other relevant locations and volcanoes mentioned in the text. Grey circles = active Holocene volcanoes (Global Volcanism Program, 2013); black triangles = volcanic sources mentioned in the text; grey shading = Brooks Range; star outlines = lakes mentioned in the text.

In 2013 sediment cores were collected from two sites at Cascade Lake using a percussion-piston coring system (long cores) and Aquatic Instruments universal corer (surface cores). Cores were split and described at the National Lacustrine Core Facility (LacCore) repository at the University of Minnesota, Twin Cities, and archive halves are housed there. The top 1.42 m of a 5.2-m-long composite sedimentary sequence, CASC-4A/2D, is the focus of this study. Analyses were limited to the upper section of the core because a) it covers the range of depths where a potential offset in ages has been reported (Steen, 2016), and b) because most well-defined distal tephra deposits in Alaska are limited to the last ~4 ka (e.g. Davies et al., 2016).

The CASC-4A/2D sediment cores were undeformed by the coring procedure and the full sequence was separated into three distinct lithologic units based on visual stratigraphy, wet bulk density, organic-matter content, and variations in magnetic parameters (Fig. S1). The new analyses reported here were made from the top 1.42 m of unit 3 (3.55-0 m), which consists of irregular millimeter- to centimeter-scale bands of silt and clay. More detailed sediment descriptions are provided by Steen (2016).

2.1 Radiometric data

Radiometric data from Cascade Lake (Steen, 2016) are summarised in Table 1. Eleven AMS ^{14}C samples analysed at the University of California-Irvine AMS Facility are reported. Samples consisted of terrestrial plant macrofossils, insect parts, resting eggs, and aquatic vegetation as available. The oldest sample analysed was from 348.5–351 cm and dates to ~15 cal ka BP. Six ^{210}Pb measurements were made from the uppermost sediment at Cascade Lake and equilibrium (~142 yr BP) is reached within the top 4 cm of the sequence.

Table 1: Radiometric ages from Cascade Lake (from Steen, 2016). Ages are reported to the nearest whole year (^{210}Pb) or five years (^{14}C) * =^{14}C ages rejected as outliers; † = samples from surface core CASC-4B, all other samples are from CASC-4A.

(a) ^{210}Pb CRS ages

Composite depth (cm)	Age (yr)	Error (yr)
0–0.5	23	1
0.5–1	48	1
1–1.5	67	2
1.5–2.25	83	2
2.25–3	112	4
3–3.5	143	7

Deleted: The 5.2-m-long composite sedimentary sequence, CASC-4A/2D, described by Steen et al. (this volume) is the focus of the age-depth model reported here, which extends down to the boundary with an underlying diamicton.…

Formatted: Heading 2

Deleted: Previous geochronological data¶ 2.1.1

Deleted: are detailed in full in Steen et al. (this volume) and

Deleted: here

Deleted: 350

Deleted: composite depth, dating

Deleted: , but as

Deleted: cores these ages are not discussed in the context of the Holocene age models. ¶

Deleted: et al., this volume

(b) ^{14}C ages

Composite depth (cm)	Sample ID (UCIAMS #)	Age (^{14}C yr)	Error (^{14}C yr)	Material dated
2.6–4.6†	147384	170	30	Resting eggs, mixed aquatic fragments
5.5–7.5	*134422**	*1765*	*20*	Insect remains, twigs, leaves, bryophyte, eggs
11–13†	147383	785	45	Leaf fragments, resting eggs, mixed aquatic fragments
30.5–32.5	131742	2825	25	Insect remains, moss fragments, resting eggs, fine unidentified pieces
85.75–87.75	128095	4160	120	Insect remains, twigs, leaves, bryophyte, resting eggs
138–140	131743	5085	20	Insect remains, moss fragments, resting eggs, fine unidentified pieces
197–199	131744	6485	25	Insect remains, moss fragments, resting eggs, fine unidentified pieces
233.5–235.5	134423	8270	35	Insect remains, twigs, leaves, resting eggs, fine unidentified pieces
245–248	*128096**	*13200*	*450*	Insect remains, aquatic vegetation, twigs, resting eggs
303–304	131745	9875	35	Insect remains, moss fragments, resting eggs, fine unidentified pieces
348.5–351	137726	12690	150	Insect fragments, twig, leaf fragments

2.2 Cryptotephra detection and analysis

The sampling and analysis of tephra for this study followed best practice guidelines (e.g. Abbott et al., 2021; Wallace et al., n.d.) to facilitate comparability with other research. No visible tephra were located in cores from Cascade Lake; in fact, no visible tephra are known north of the Brooks Range. Targeted cryptotephra analyses were undertaken using contiguous 1-cm-thick subsamples from 1.42 m composite depth to the surface. Standard methods (e.g. Blockley et al., 2005) were used to produce glass shard concentration profiles throughout the two core sections. Samples were sieved using 20 micron nylon mesh and the heavy liquid, lithium heteropolytungstate (LST), was used for density separations.

Glass shard morphologies and grain sizes were recorded using optical microscopy and images of the processed samples (i.e. grains that are >20 µm and <2.45 g cm^{-3}, mounted in Canada Balsam). Shard depths were estimated by recording the number of 3µm fine-focus increments required to focus through individual grains. Other grain size measurements (e.g. axis lengths, perimeter, maximum projected area) were calculated using ImageJ software. Values for maximum axis length are reported, as well as geometric size (d_v) and sphericity (ψ) (calculated following the methods reported in Saxby et al., 2020). As only a small number of measurements were made due to low concentrations of glass present in the sample slides (7–15 shards/sample; Table S1), these measurements are not fully representative of their source eruptions. For example, Saxby et al. (2020) recommend that 50–500+ measurements are used to characterise mean and maximum shard sizes, respectively. However, these quantitative characterisations are reported here as preliminary data for distal deposits of these tephra.

Deleted: -
Deleted: -
Deleted: -
Deleted: -
Deleted: -
Deleted: -
Deleted: -
Deleted: -
Deleted: -
Deleted: -
Deleted: -
Deleted: ¶
I1
... [1]
Deleted: The ages of tie-points from the geometric field models are based on a database of 75 selected sedimentary palaeomagnetic records from the SED12k data compilation (Donadini et al., 2010; used by CALS10k.1b, Korte et al., 2011). The database was further parsed to exclude bulk ^{14}C samples, archaeomagnetic data with large temporal uncertainties, and palaeomagnetic behaviour incompatible with the majority of records during the Holocene (pfm9k.1b, Nilsson et al., 2014). Both models have reported estimated temporal resolutions of ± 500 a. Burial Lake tie-point ages and errors are derived from the ^{14}C age model of the sediment cores (Dorfman, 2013), which is based on terrestrial macrofossils and shows remarkably linear sediment accumulation over ~ 17 ka cal BP.¶
2.3
Deleted: Cryptotephra analyses are reported here from the past 4 ka, as a large number of the most well-known, dated, and widely distributed tephra in Alaska were erupted during this time period (Davies et al., 2016). This is also the interval when the ^{14}C ages in Cascade Lake cores appear to be too old relative to the expected ages of the PSV features and therefore where tephra have significant potential to validate and improve a final age-depth model.¶
No visible tephra were located in cores from Cascade Lake (in fact, no visible beds are known north of the Brooks Range); targeted…
Deleted: Lithium Heteropolytungstate

Glass shards for geochemical analysis were re-extracted from peaks in shard concentration using heavy liquid separation. After rinsing, the remaining sample material was pipetted into a pre-drilled hole in an acrylic puck (fixed onto a flat glass plate with double sided tape) and covered with epoxy resin. Once cured, the flat puck surface was then lightly polished to expose glass surfaces and carbon coated prior to electron probe microanalysis (EPMA). Individual glass shards were analysed on a JEOL 8900 Superprobe at the University of Alberta by wavelength dispersive X-ray spectroscopy (WDS) following established protocols (e.g. Jensen et al., 2008, 2019).

A standard suite of ten elements (Si, Ti, Al, Fe, Mn, Mg, Ca, Na, K, Cl; 30 second peak count times; ZAF correction method) was measured using a 5 µm beam with 15 keV accelerating voltage and 6 nA beam current. This focussed beam (usually 10 µm is utilised) can result in Na loss in more sensitive glasses. However, where intensity data loss does occur, it has been shown that empirical corrections can be applied if the data demonstrate linear variance over time (Nielsen and Sigurdsson, 1981). Here Na, and if necessary, Si, were corrected for Time Dependent Intensity (TDI) loss (or gain) using a self-calibrated correction with Probe for EPMA software (Donovan et al., 2015). This method at these settings has been successfully applied in several studies on tephra of different compositions and grain-sizes (Foo et al., 2020; Jensen et al., 2019, 2021).

Two secondary standards of known composition were run concurrently with all tephra samples: ID 3506, a Lipari rhyolite obsidian, and a reference sample of Old Crow tephra, a well-characterised, secondarily hydrated tephra bed (Kuehn et al., 2011). All results were normalised to 100% and are presented as weight percent (wt%) oxides. New major-element geochemical data and associated standard measurements, as well as data points for relevant reference material (analysed concurrently, where possible), are reported in the Supplementary Information (Tables S2, S3). Non-glass analyses (e.g. minerals, biogenic silica) and analyses with analytical totals <94% were rejected but are available in Table S2.

Correlations to known tephra or volcanic sources were based on major-element geochemistry (including concurrent re-analyses with reference materials where possible), stratigraphic position and consistent glass morphological characteristics.

2.3 Bayesian age modelling

Three steps are detailed here for identifying and resolving problematic chronometer offsets using the radiometric data from Steen (2016) and new cryptotephra correlated ages.

Deleted: and samples were mounted

Deleted: puck and

Deleted: before being

Deleted: New data are reported here from

Deleted: (e.g. Jensen et al., 2019; Foo et al., 2020).

Deleted: (e.g.

Deleted: S1, S2).

Deleted: 4

Both manual approaches and statistical outlier analysis techniques included in OxCal v4.4 (Bronk Ramsey, 2009a, 2009b) are applied in the following order.

Firstly, ages that were obviously out of stratigraphic sequence (previously highlighted by Steen, 2016) were rejected. Secondly, OxCal's Poisson process model (P_Sequence, Bronk Ramsey, 2008) was used to construct independent models for each chronometer. IntCal20 (Reimer et al., 2020) and Bomb21NH1 (Hua et al., 2021) were used for ^{14}C calibrations as appropriate. The independent models were visually compared to detect offsets between the dating methods. This is an effective preliminary check of the data, especially where there is an imbalance between the number and the resolution of dates used from each chronometer, which may bias statistical outlier analysis techniques. For example, ^{210}Pb and ^{14}C ages from Davies et al. (2018) were initially assessed using OxCal's agreement indices (AI) and showed strong agreement for ^{210}Pb dates (19–43 ages/site with age ranges of 2–10 years) and poor agreement for ^{14}C dates (4–7 ages/site for the same period, with age ranges of to 130 calibrated years), even though the ^{14}C data were found to be accurate as the ^{210}Pb data were systematically offset. Here, ^{210}Pb dates from 0–3.5 cm are used to check for agreement with the uppermost ^{14}C age (2.6–4.6 cm) and cryptotephra isochrons are used as independent checks on the remaining Late Holocene ^{14}C ages.

Finally, the remaining chronological data were combined in one composite P_Sequence model (OxCal v4.4; Bronk Ramsey, 2009a). This set-up allows variable accumulation rates; here the k parameter (deposition events defined as increments per unit length, controlling model rigidity and resolution) was set as variable rather than fixed to increase model flexibility (Bronk Ramsey and Lee, 2013). Outliers were judged statistically using OxCal's agreement indices (AI), which show the extent to which the modelled posterior distributions overlap with the original distributions, and general (Student's t) outlier analysis to identify any remaining anomalous ages in the parsed dataset (Bronk Ramsey, 2009b). All ages were given the prior probability of 5% of ages being incorrect; if an age needs to be shifted substantially (by more than two standard deviations) to fit the resulting age-depth model it was identified as an outlier and downweighed in the process (Blockley et al., 2007).

3 Cryptotephra abundance and geochemical data

Deleted: Steen et al. (this volume) and new cryptotephra correlated ages. Firstly, ages that were obviously out of stratigraphic sequence were rejected previously by Steen et al. (this volume)….

Deleted: These were then visually compared to detect offsets between the dating methods. This is more effective than using statistical techniques as a first approach as they can be biased by datasets with high numbers of dates and tight distributions. Here, cryptotephra isochrons were used as independent checks for the other chronological methods, e.g. to identify ^{14}C outliers. …

Deleted: resulting

Deleted: Bronk Ramsey, 2009).

Deleted: (Bronk Ramsey, 2013). General (Student's t) outlier analysis was used to identify any remaining anomalous ages in the parsed dataset. All

Glass shards were present in ~75% of the samples analysed in this study (108/143 total samples). The composite shard concentration profile for the 1.42 m of core samples analysed here is shown in Fig. 2. Twenty-eight peaks were chosen for geochemical analysis based on the relative abundances of shards counted at those depths. This generally was around 4–42 shards/gram, except for the top 0–1 cm, which had 88 shards/gram. For each sample, geochemical analyses were performed on single grains, but 15 of the peaks chosen resulted in fewer than five shards exposed on the EPMA puck surface. This is likely due to the relatively low concentrations of glass present overall.

Fig. 2

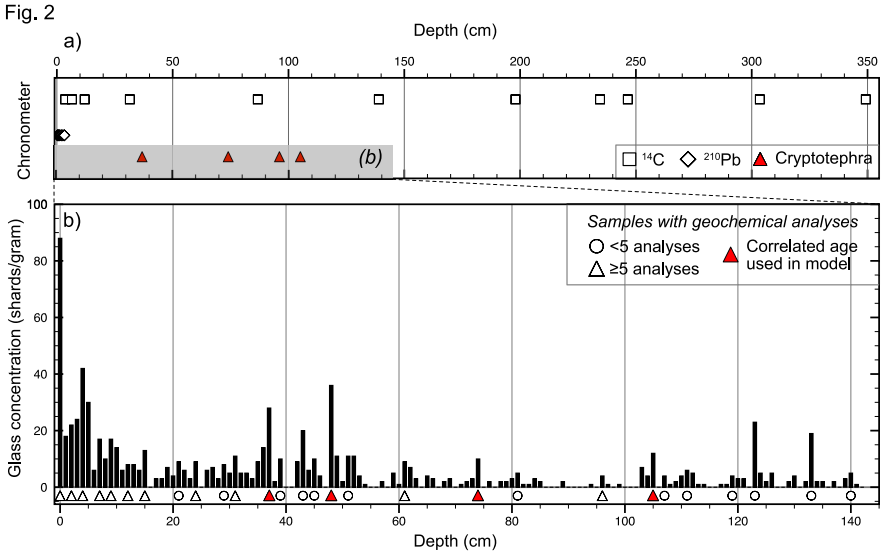

Figure 2: Cascade Lake core CASC-4A/2D ensemble chronological controls. (**a**) The composite depths of radiometric ages (^{14}C and ^{210}Pb; Table 1) and correlated cryptotephra ages (Table 4). The shaded grey area shows the depth interval of core sampled for cryptotephra analysis (expanded in panel b). (**b**) Glass shard concentration counts produced down to 1.42 m, and the composite depths of analysed glass peaks. Twenty-eight out of one hundred and forty-two samples were geochemically analysed: circles = <5 points analysed; triangles = >5 points analysed; filled red triangles have correlated ages that are used in the age-depth model.

Of the remaining 13 samples, five have dominant unique geochemical populations (i.e. primary deposits, likely relating to a single eruption, are strongly represented), six have multiple identifiable trends/populations (representing an amalgamation of shards from multiple eruptions), and two have sparse shards with no discernible geochemical trends. Table 3 and Figure 3 show the samples analysed, the average major-element data for identified geochemical populations, and any geochemical correlations to known eruptions with associated chronological data or similarities to known volcanic sources. Normalised

Deleted: here.
Deleted: counted
Deleted: single eruptions
Deleted:)
Deleted: Fig.
Deleted:
Deleted: EPMA

single point major-element geochemical data and associated standard analyses are provided in Tables S2 and S3.

The shard profile shows multiple closely spaced peaks and tails (Fig. 2) that translates into several samples containing multimodal geochemical populations, especially in the top 30 cm of the core profile. This could be evidence for taphonomic problems (e.g. reworking, bioturbation), but a lack of evidence for sediment reworking and an abundance of eruptions in the late Holocene suggest this is not a substantial problem at Cascade Lake (see section 5.1.1 below for detailed discussion).

3.1 Unique glass populations

Five of the analysed samples contained glass shards that show dominant unimodal rhyolitic geochemical populations based on between 10 and 36 individual point analyses. These are interpreted as primary tephra-fall events relating to contemporaneous eruptions. Grain size data were measured for 7 to 15 shards per sample and show that average maximum axis length and sphericity values are very similar for all five samples (23-27 microns and 0.56-0.63 respectively). Four of these five samples can be used as isochrons as they correlate to reference material from known and dated eruptions (University of Alberta reference collection samples, Fig. 3; details provided in Tables 3 and S2). Key information regarding these eruptions and the tephra deposits are summarised in Table 4. Grain size data and shard images are presented in the supplementary files (Table S1, Fig. S2). Samples are discussed here individually from oldest to youngest and previously published age estimates are given as two sigma ^{14}C calibrated age ranges unless otherwise stated.

Deleted:
Deleted: EPMA datasets
Deleted: S1
Deleted: S2
Deleted: 38 geochemical
Deleted: (i.e. they
Deleted: no evidence of secondary reworking
Deleted: S1

Table 3: Normalised average major element geochemical glass data for identifiable populations of analysed tephra samples and suggested correlations. Popn: unimodal geochemical data are labelled as '-'; where multiple geochemical populations are identified, they are labelled separately (e.g., a, b), but if they are interpreted as being related heterogenous populations a combined average is also shown (e.g., a+b). FeOt = total iron oxide as FeO; H_2O_d = water by difference; numbers listed in brackets = 1 S.D. (**a**) Samples used here as tie-points; (**b**) Reference material analysed at the University of Alberta, for full details regarding the original sample details please see listed references. (**c**) Samples with multiple populations or too few points to use as tie-points. Only groups of 3 or more analyses are shown here – for full details see Table S2.

a) Samples used as tie-points

Sample #	Popn	SiO_2	TiO_2	Al_2O_3	FeOt	MnO	MgO	CaO	Na_2O	K_2O	Cl		H_2Od	n	Correlation
CL-37	-	76.73	0.11	13.27	0.60	0.08	0.12	0.77	4.39	3.83	0.12		3.90	10	Opala (OP)
		(0.26)	(0.03)	(0.12)	(0.09)	(0.03)	(0.02)	(0.04)	(0.23)	(0.22)	(0.02)		(1.31)		
CL-48	a	74.52	0.22	14.12	1.49	0.06	0.34	1.57	4.07	3.35	0.34		2.23	10	
		(0.58)	(0.06)	(0.32)	(0.20)	(0.01)	(0.08)	(0.13)	(0.27)	(0.25)	(0.03)		(1.58)		Mt. Churchill –
	b	77.76	0.16	12.43	1.06	0.04	0.15	0.91	3.65	3.61	0.30		2.25	12	White River Ash
		(0.69)	(0.05)	(0.42)	(0.10)	(0.02)	(0.04)	(0.18)	(0.16)	(0.19)	(0.04)		(1.89)		(northern lobe,
	a+b	76.29	0.19	13.20	1.26	0.05	0.24	1.21	3.84	3.49	0.31		2.24	22	WRAn)
		(1.77)	(0.06)	(0.94)	(0.26)	(0.02)	(0.11)	(0.37)	(0.30)	(0.25)	(0.04)		(1.71)		
CL-74	-	74.16	0.30	13.91	1.96	0.11	0.46	2.18	4.81	1.91	0.25		0.48	36	Ruppert
		(0.63)	(0.05)	(0.23)	(0.15)	(0.02)	(0.06)	(0.14)	(0.26)	(0.09)	(0.03)		(1.24)		
CL-96	-	74.04	0.40	13.72	1.89	0.08	0.49	2.06	4.33	2.81	0.24		0.86	12	Unknown
		(0.95)	(0.03)	(0.46)	(0.15)	(0.02)	(0.09)	(0.18)	(0.23)	(0.08)	(0.02)		(1.18)		
CL-105	a	71.10	0.48	15.19	2.34	0.13	0.52	1.64	5.53	2.91	0.20		0.54	11	Aniakchak CFE II
		(0.29)	(0.03)	(0.15)	(0.07)	(0.02)	(0.03)	(0.04)	(0.23)	(0.12)	(0.02)		(0.93)		

b) Reference material analyses from the University of Alberta

Site	Sample ID	SiO_2	TiO_2	Al_2O_3	FeO_t	MnO	MgO	CaO	Na_2O	K_2O	Cl		H_2O_d	n	Correlation	Reference sample details
Duke River Fan, YT	UA 1044	74.32	0.21	14.18	1.54	0.06	0.32	1.67	4.11	3.26	0.33		2.40	55	White River	
		(0.63)	(0.05)	(0.33)	(0.15)	(0.03)	(0.05)	(0.16)	(0.18)	(0.13)	(0.04)		(1.15)		Ash (northern lobe)	Jensen (2007)
Sixtymile River area, YT	UT 1480, Sample 16	73.95	0.21	14.38	1.50	0.06	0.35	1.77	4.29	3.23	0.34		2.82	31	White River Ash (northern lobe)	Preece *et al.* (2014), this paper
		(2.06)	(0.07)	(0.99)	(0.31)	(0.03)	(0.14)	(0.49)	(0.31)	(0.19)	(0.04)		(0.78)			
	UT 1482, Sample 17	73.65	0.23	14.50	1.59	0.06	0.38	1.83	4.26	3.25	0.34		3.06	34		
		(1.80)	(0.06)	(0.87)	(0.29)	(0.02)	(0.12)	(0.46)	(0.26)	(0.19)	(0.05)		(0.88)			
Zagoskin Lake, AK	UA 1602a	59.13	1.40	16.45	7.50	0.22	2.97	6.06	4.61	1.57	0.13		2.30	17	Aniakchak CFE II (andesite, rhyodacite)	*Ager* (2003); *Davies et al.* (2016)
		(0.97)	(0.07)	(0.16)	(0.64)	(0.03)	(0.22)	(0.40)	(0.26)	(0.11)	(0.02)		(1.07)			
	UA 1602b	71.07	0.50	15.19	2.55	0.14	0.51	1.78	5.07	3.05	0.19		2.48	32		
		(0.52)	(0.05)	(0.28)	(0.2)	(0.03)	(0.08)	(0.19)	(0.29)	(0.13)	(0.02)		(1.56)			
Ruppert Lake, AK	UA 2557	74.08	0.30	13.96	2.00	0.10	0.46	2.18	4.80	1.93	0.22		0.53	17	Ruppert	*Monteath et al.* (2017)
		(0.39)	(0.05)	(0.16)	(0.12)	(0.03)	(0.04)	(0.10)	(0.14)	(0.10)	(0.02)		(0.90)			
Southern Kamchatka	UA 3286	76.65	0.12	13.31	0.69	0.11	0.12	0.77	4.24	3.91	0.11		2.65	30	Opala (Phase	*Andrews et al.* (2018)
		(0.20)	(0.04)	(0.12)	(0.03)	(0.03)	(0.02)	(0.03)	(0.11)	(0.09)	(0.02)		(0.71)		III)	

c) Other samples analysed

Sample	Popn	SiO2	TiO2	Al2O3	FeOt	MnO	MgO	CaO	Na2O	K2O	Cl		H2Od	n
CL-0	a	71.02	0.48	14.90	2.36	0.16	0.50	1.67	5.64	3.09	0.23		1.46	7
		(0.29)	(0.03)	(0.15)	(0.08)	(0.03)	(0.02)	(0.05)	(0.26)	(0.08)	(0.03)		(1.26)	
	b	74.42	0.16	13.99	1.28	0.05	0.32	1.57	4.63	3.33	0.33		3.12	3
		(1.46)	(0.04)	(0.76)	(0.28)	(0.02)	(0.12)	(0.29)	(0.13)	(0.12)	(0.01)		(1.59)	
	c	74.68	0.32	13.68	2.02	0.09	0.46	2.22	4.43	1.94	0.21		1.78	6
		(0.84)	(0.04)	(0.67)	(0.16)	(0.02)	(0.04)	(0.19)	(0.34)	(0.05)	(0.06)		(0.62)	
	d	75.63	0.26	13.51	1.22	0.05	0.31	1.30	4.54	3.05	0.15		2.32	6
		(1.35)	(0.10)	(0.44)	(0.41)	(0.01)	(0.10)	(0.38)	(0.45)	(0.19)	(0.07)		(1.05)	
	e	76.91	0.33	12.27	1.57	0.03	0.26	1.16	4.33	2.97	0.21		1.61	3
		(0.45)	(0.04)	(0.09)	(0.11)	(0.01)	(0.02)	(0.02)	(0.33)	(0.01)	(0.01)		(0.48)	
CL-2	a	71.00	0.49	15.00	2.48	0.14	0.52	1.68	5.42	3.11	0.22		1.35	14
		(0.59)	(0.10)	(0.23)	(0.34)	(0.03)	(0.10)	(0.20)	(0.16)	(0.14)	(0.03)		(0.78)	
	b	73.73	0.21	14.46	1.51	0.04	0.37	1.77	4.52	3.13	0.33		2.81	5
		(0.35)	(0.02)	(0.23)	(0.05)	(0.03)	(0.03)	(0.10)	(0.12)	(0.08)	(0.02)		(1.14)	
	c	74.17	0.32	13.75	1.94	0.12	0.45	2.20	4.82	2.03	0.26		1.14	4
		(0.45)	(0.03)	(0.16)	(0.08)	(0.02)	(0.01)	(0.18)	(0.23)	(0.04)	(0.01)		(0.74)	
	d	75.86	0.25	13.18	1.56	0.07	0.31	1.66	4.96	2.01	0.17		2.04	4
		(0.27)	(0.04)	(0.14)	(0.05)	(0.03)	(0.04)	(0.11)	(0.14)	(0.03)	(0.02)		(0.28)	
	e	76.90	0.26	12.63	1.19	0.07	0.22	1.05	4.20	3.35	0.18		3.07	5
		(1.24)	(0.16)	(0.35)	(0.52)	(0.02)	(0.12)	(0.38)	(0.23)	(0.34)	(0.11)		(0.93)	
CL-4	a	66.61	0.77	15.68	4.45	0.13	1.19	3.50	4.88	2.63	0.20		1.79	4
		(1.64)	(0.26)	(0.22)	(1.07)	(0.05)	(0.14)	(0.44)	(0.3)	(0.12)	(0.11)		(0.79)	
	b	70.86	0.49	15.00	2.47	0.14	0.51	1.69	5.50	3.17	0.22		1.09	15
		(0.86)	(0.04)	(0.17)	(0.35)	(0.03)	(0.08)	(0.18)	(0.36)	(0.3)	(0.02)		(0.91)	
	c	76.71	0.12	13.26	0.61	0.12	0.09	0.72	4.25	4.07	0.10		2.78	3
		(0.16)	(0.04)	(0.02)	(0.17)	(0.03)	(0.06)	(0.03)	(0.18)	(0.36)	(0.04)		(0.86)	
CL-7	a	70.93	0.48	15.03	2.36	0.13	0.59	1.88	5.40	3.03	0.20		1.04	5
		(0.19)	(0.02)	(0.12)	(0.09)	(0.04)	(0.13)	(0.38)	(0.45)	(0.20)	(0.03)		(0.15)	
	b	75.83	0.23	13.31	1.55	0.07	0.33	1.67	4.82	2.06	0.16		1.63	6
		(0.61)	(0.05)	(0.39)	(0.04)	(0.03)	(0.08)	(0.24)	(0.23)	(0.1)	(0.04)		(0.62)	
CL-31		77.92	0.13	12.22	1.06	0.06	0.15	0.85	3.84	3.53	0.31		1.97	6
		(0.7)	(0.02)	(0.55)	(0.1)	(0.03)	(0.04)	(0.23)	(0.34)	(0.26)	(0.01)		(1.16)	
CL-61	a	71.23	0.43	15.05	2.39	0.15	0.44	1.57	5.50	3.09	0.20		-0.28	3
		(0.80)	(0.04)	(0.28)	(0.07)	(0.02)	(0.05)	(0.13)	(0.56)	(0.19)	(0.02)		(0.28)	
	b	77.70	0.21	12.72	1.23	0.05	0.34	2.05	4.01	1.62	0.10		0.44	4
		(0.33)	(0.02)	(0.20)	(0.07)	(0.03)	(0.01)	(0.05)	(0.16)	(0.09)	(0.02)		(1.40)	
CL-105	b	71.81	0.51	14.75	2.32	0.10	0.41	1.43	4.85	3.69	0.17		0.37	4
		(0.55)	(0.09)	(0.03)	(0.22)	(0.02)	(0.05)	(0.13)	(0.22)	(0.04)	(0.01)		(0.14)	

Deleted: ¶ ... [5]
Formatted ... [6]
Deleted: Total
Deleted: 100.00
Deleted: (0.00)
Deleted: 100.00
Deleted: (0.00)
Deleted: 100.00
Deleted: (0.00)
Deleted: 100.00
Deleted: (0.00)
Deleted: 100.00
Deleted: (0.00)
Deleted: 100.00
Deleted: (0.00)
Deleted: 100.00
Deleted: (0.00)
Deleted: 100.00
Deleted: (0.00)
Deleted: 100.00
Deleted: (0.00)
Deleted: 100.00
Deleted: (0.00)
Deleted: 100.00
Deleted: (0.00)
Deleted: 100.00
Deleted: (0.00)
Deleted: 100.00
Deleted: (0.00)
Deleted: 100.00
Deleted: (0.00)
Deleted: 100.00
Deleted: (0.00)
Deleted: 100.00
Deleted: (0.00)
Deleted: 100.00
Deleted: (0.00)
Deleted: 100.00
Deleted: (0.00)
Deleted: 100.00
Deleted: (0.00)

Table 4: Cascade Lake cryptotephra and their suggested correlative eruptions. Radiocarbon modelled age estimates produced in this paper for the core depth of the cryptotephra are compared with published ages for the listed eruptions. Bayesian modelled ages for both Aniakchak CFE II and Opala are updated here using OxCal v4.4 (Bronk Ramsey, 2009a) and IntCal20 (Reimer et al., 2020).

Sample (Lab #)	Suggested correlation		Cascade Lake ^{14}C age (cal yr BP)		Age estimate for correlated eruption			
	Tephra	Source volcano			95% range (cal yr BP)	Method	Deposit type	Age estimate reference(s)
CL-37 (UA3721)	OP	Opala, Kamchatka	3300–2800		1395–1305	Calibrated ^{14}C (IntCal20)	Visible tephra (Kamchatka)	Braitseva et al. (1995); updated here using IntCal20
CL-48 (UA3730)	WRAn	Mt. Churchill, Alaska	3780–2980		1689–1540	Calibrated ^{14}C (IntCal20)	Visible tephra (Alaska, Yukon)	Reuther et al. (2020)
CL-74 (UA3733)	Ruppert	Unknown (likely Alaska)	4595–3700		2800–2130	Calibrated ^{14}C (IntCal20)	Distal cryptotephra (four bogs - Newfoundland, Canada; Maine, Michigan, New York, USA)	Jensen et al. (2021)
CL-96 (UA3735)	-	Unknown	5130–4380		-	-	-	-
CL-105a (UA3736)	CFE II	Aniakchak, Alaska	5375–4575		3590–3545	Calibrated ^{14}C (IntCal20) & ice core	Visible tephra (Alaska) and cryptotephra (Alaska, USA; Newfoundland, Canada)	Davies et al. (2016); updated here using IntCal20
					3572 ± 8	GICC05 (with correction)	Distal cryptotephra (North Greenland Ice Core Project, NGRIP, Greenland)	Vinther et al. (2006); Adolphi & Muscheler (2016); Pearce et al. (2017)
					(-19 ± 3)			

Deleted: estimates (95% range
Deleted: ^{14}C (cal yr BP)
Deleted: PSV-1 (yr BP)
Deleted: 3180-2300
Deleted: 1720-990
Deleted: -
Formatted: Font colour: Auto, English (UK)
Deleted: 3895-2935
Formatted: Font colour: Auto, English (UK)
Deleted: 2110-1360
Deleted: -
Deleted: 2795-2280
Deleted: -
Deleted: submitted
Deleted: 4920-4145
Deleted: 5345-4840
Deleted: 3355-2600
Deleted: -
Deleted: 5460-5030
Deleted: 3525-2675
Deleted: -

Fig. 3

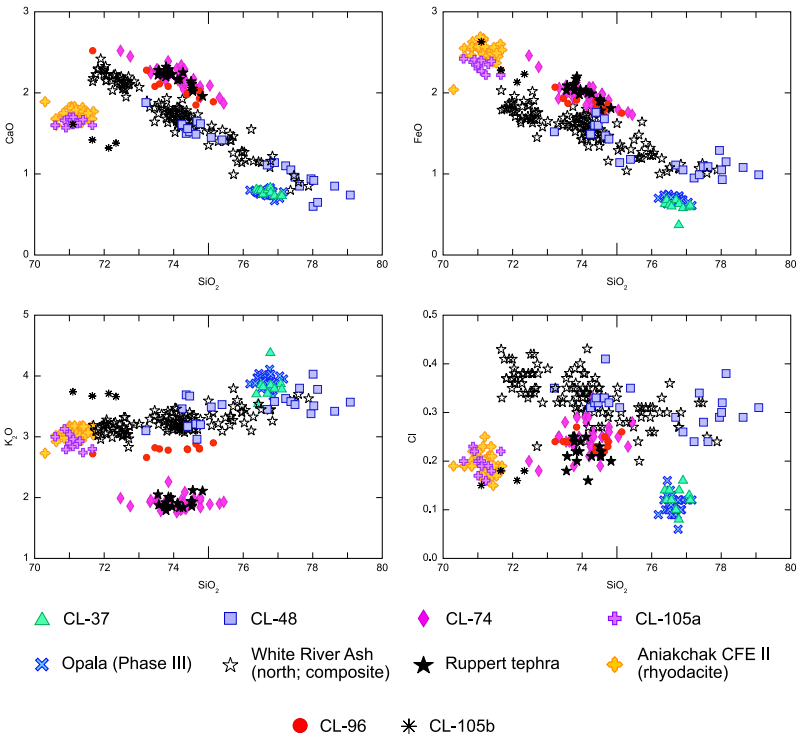

Figure 3: Geochemical biplots showing major element data for the five unique populations of cryptotephra glass identified from Cascade Lake sediment, and data for reference material where relevant. Points for CL-105b are also plotted, for reference. See Table 3 for sample details and Table S2 for individual point data.

3.1.1 CL-105 (Aniakchak Caldera Forming Eruption II)

CL-105, a peak concentration of 12 shards/gram, is characterised by platy and cuspate shards. It is a geochemical match for the dominant rhyodacite population of the widespread Late Holocene caldera forming eruption of Aniakchak (CFE II) (Fig. 3; see Bacon et al., 2014; Neal et al., 2001; Riehle et al., 1987 for details). Tephra from this eruption have been found visibly across southern and western Alaska, and as cryptotephra in the Bering Sea, Yukon, Newfoundland and Greenland (Davies, 2018; Denton and Pearce, 2008; Pearce et al., 2017, 2004; Ponomareva et al., 2018; Pyne-O'Donnell et al., 2012). A small second population of four points was also identified in this sample (CL-105b, Table 3c); they do not

Deleted: **Table 4:** Cascade Lake cryptotephra and their suggested correlative eruptions. Age estimates for the core depth of the cryptotephra from Steen et al. (this issue) are compared with published ages for the listed eruptions. Bayesian modelled ages for both Aniakchak CFE II and Opala are updated here using OxCal and IntCal20.¶
¶
<object>

Deleted: S1

Deleted: Bacon et al., 2014; Neal et al., 2001; Riehle et al., 1987).

correlate with reference material for this eruption (e.g. Wallace et al., 2017) but it is unclear if these represent a separate event or shards from the main population with alkali loss.

Chronologically, the Aniakchak CFE II tephra has disparate age estimates where modelled radiocarbon dates and ice core ages are notably offset (see Davies et al., 2016, for a detailed summary of references). Radiocarbon age estimates have been produced from sequences with visible tephra as well as distal lakes and peat bogs with correlated cryptotephra. A precise ice-core model age estimate is associated with distal cryptotephra identified in North Greenland Ice Core Project (NGRIP) samples.

The identification of an eruption event in NGRIP is supported using geochemically correlated glass shards and sulphate peaks (Coulter et al., 2012; Pearce et al., 2004). Additional evidence for the eruption is also provided by tree ring perturbations during in this interval (Baillie and McAneney, 2015), which have been correlated to the NGRIP records. Geochemically correlated glass shards in two NGRIP intervals have overlapping GICC05 modelled ages of 3594–3589 yr BP (1641–1639 BCE - QUB-1198, 1644–1643 BCE - QUB 1201; Coulter et al., 2012; Vinther et al., 2006). Differences in the IntCal13 and GICC05 timescales over the Holocene were quantified by a transfer function developed by Adolphi and Muscheler (2016), using common variations in ^{14}C and ^{10}Be production rates (recorded in tree-rings and ice cores respectively). If their correction factor for this time interval (-19 ± 3 a) is applied to the GICC05 chronology, the resulting NGRIP modelled age for the eruption is 3572 ± 4 cal yr BP (1 S.D.; Adolphi and Muscheler, 2016; Pearce et al., 2017).

Here we report updated modelled eruption ages produced using the Tau_Boundary function in OxCal v.4.4 (Bronk Ramsey, 2009a) with IntCal20 (Reimer et al., 2020) following Davies et al. (2016; Fig. S3, see Table S4 for details). The Tau_Boundary function is used here for both the upper and lower boundaries around a single-phase eruptive event. All dates associated with the tephra are included in the model, with an exponential rise and fall before and after the eruption event (i.e. assuming that dates cluster closely around the event). For Aniakchak CFE II, the ice-core modelled age discussed above is only compatible with published ^{14}C ages if two of the three ^{14}C ages that underlie the tephra in an exposed peat section in northwest Alaska (Blackford et al., 2014) are removed as outliers. This is unexpected because the peat section is one of the most precisely dated terrestrial sequences for Aniakchak CFE II, with six samples analysed at 0.5 cm increments over 3 cm

Deleted: A second population of four points was also identified in this sample (CL-105b, Table 3c), however it is unclear if these represent a separate event or alkali loss from the main population…

Deleted: Chronologically, Aniakchak CFE II has been dated with radiocarbon from sequences with visible tephra and distal lakes and peat bogs with correlated cryptotephra, as well as with a precise ice-core model age estimate from distal cryptotephra identified in Greenland ice cores. The latter is supported using geochemically correlated glass shards as well as sulphate peaks and tree ring perturbations recorded in this interval (Coulter et al., 2012; McAneney and Baillie, 2019; Pearce et al., 2004). Glass shards correlated to the eruption in two NGRIP intervals have overlapping associated ice-core modelled ages of 3594-3589 yr BP (1641-1639 BCE – QUB-1198, 1644-1643 BCE –…

Deleted: When a correction factor of -19 ± 3 a

Deleted: (Adolphi and Muscheler, 2016)

Deleted: (Pearce et al., 2017).

Deleted: with IntCal20 (

Deleted: Davies et al., 2016; Fig. S1, see Table S4 for details). The ice-core chronology…

immediately surrounding the tephra. While there are no obvious reasons for disregarding these two ages, beyond the disagreement with the ages from the ice cores, in this instance it seems pertinent to do so. Modelled Tau_Boundary estimates for the eruption age are: a) 3545–3425 cal yr BP when all ^{14}C dates are included, b) 3610–3450 cal yr BP with two ^{14}C dates removed, and c) 3590–3545 cal yr BP including all but two ^{14}C dates and the NGRIP ice core chronology age (Fig. S3). At Cascade Lake, using either the ice core chronology age estimate of 3572 ± 4 cal yr BP (Adolphi and Muscheler, 2016; Pearce et al., 2017) or the Tau_Boundary model age (c, above) for Aniakchak CFE II shows that this age is younger than the radiometric age-model estimate for this depth by ~1000–1800 years (Table S5).

Deleted: -
Deleted: -
Deleted: -
Deleted: S1
Deleted: while neither estimated age for this depth from Steen et al. (this volume) overlaps here, the PSV-1 age model is substantially closer than the ^{14}C age model (Table 4…

3.1.2 CL-96 (unknown)

CL-96 represents a small peak of only four shards/gram but analytical points were obtained from 10 individual shards. These data show relatively high values for wt% TiO_2, FeO and CaO (Table 3a) and are similar to CL-74 for many major elements but have substantially higher wt.% K_2O (2.81 wt.% average vs. 1.91 wt.%, respectively). The shards are likely from a source in Alaska and the Aleutian Arc and are similar to published average analyses for glass from the Katmai volcanic cluster (Fierstein, 2007) but cannot be directly correlated here to a particular vent or eruption. Therefore, there are no associated age estimates that can be used here to compare with other Cascade Lake chronometers. For future comparisons, the few observed shards from CL-96 were typically chunky with a small number of vesicles or cuspate edges and the final age-model estimate for this depth is 3550–2920 cal yr BP (2 sigma; Table S6).

Deleted: yielded 10
Deleted: that have
Deleted:). These analyses
Deleted: ,

3.1.3 CL-74 (Ruppert tephra)

CL-74 has a shard concentration peak of 10 shards/gram but a disproportionately high number of analyses (38) when compared to other samples. This rhyolitic glass population of platy and cuspate shards has relatively low wt.% K_2O values (~2.0%) compared to most other known tephra from Alaska and is a geochemical match for the Ruppert tephra. This tephra was first identified in Newfoundland (NDN-230; Pyne-O'Donnell et al., 2012) and tentatively correlated to Augustine G tephra, although this is now known to be incorrect (Blockley et al., 2015; Monteath et al., 2017). While it is geochemically similar to glass from

Deleted: distinctly

Augustine volcano, no proximal correlative is currently known. The tephra was later found in, and subsequently named after, Ruppert Lake, directly south of Cascade Lake on the southern slope of the Brooks Range (Monteath et al., 2017) and has also been identified in peatlands in the Yukon (Davies, 2018) and eastern USA (Jensen et al., 2021).

It is an unusual situation to have a distal tephra deposit correlated between multiple sites that are located up to 5000 km apart but with no identified visible deposits. Such a correlation relies heavily on the geochemical characterisation and coincident timing. While there was some uncertainty about the validity of the geochemical correlation between sites from previously published data that were analysed at different times, this has recently been addressed with concurrently analysed samples from Alaska and the eastern USA and Canada by Jensen et al., (2021). Regardless of where Ruppert tephra is sourced from, we are confident in this correlation to Cascade Lake, as Ruppert tephra has been reported (and named) in this region and its presence in Alaska is firmly established.

Chronologically, the ^{14}C age models from Ruppert Lake, Alaska, show some evidence of old carbon contamination (core RS: 3230-2930 cal yr BP, core RC: 2920-2520 cal yr BP, Monteath et al., 2017) and these are therefore not interpreted as accurate for constraining the eruption age. Instead, our recommended best age estimate is a modelled ^{14}C age of 2800–2130 cal yr BP (two-sigma; Jensen et al., 2021) produced from distal deposits in four peat bogs (located in Newfoundland, Canada; Maine, Michigan and New York, USA). This age is younger than the radiometric age-model estimate for this depth at Cascade Lake by ~1240–2130 years (Table S5).

3.1.4 CL-48 (White River Ash, northern lobe)

CL-48 is the largest glass concentration peak of the pre-19th century sequence, with 36 shards/gram. These vesicular to frothy rhyolitic glass shards typically contain large numbers or microlites inclusions. They are geochemically similar to the White River Ash, which comprises two Late Holocene eruptions from Mt. Churchill (Lerbekmo, 2008; Preece et al., 2014). Major element glass geochemical data for these eruptions are very similar (with substantial overlap) but given the geographic relationship to the main plume directions, broad range of wt.% SiO_2 values and bimodal geochemistry of CL-48 shards, it likely correlates with the older northern-focused eruption (WRAn). The tephra from this eruption is more

Deleted: Mt.
Field Code Changed
Deleted: submitted
Deleted: Ruppert Lake's
Deleted: model shows
Deleted: but Jensen et al. (submitted) produced
Deleted: two-sigma
Deleted: -
Deleted: using ^{14}C ages
Deleted: four
Deleted: agrees well with Steen et al.'s (this volume) PSV-1
Deleted: 4
Deleted: pumaceous

geochemically diverse than that of the younger eastern lobe (Davies et al., 2019) and is preserved as a visible bed in sediment deposits north of the vent in Alaska and the Yukon.

Reference geochemical data from three WRAn samples in the Yukon (Jensen, 2007; Preece et al., 2014) are plotted in Fig. 3 to demonstrate the observed variability; distal correlatives trend towards higher wt.% SiO_2 values compared to proximal samples. While geochemical differences between sites may tend to preclude a correlation, available analyses show that distal WRAn does vary geochemically by geographic location, although the entire geochemical trend is present more proximal to the volcano. Whether this is the result of a layered magma chamber or multiple, closely spaced eruptions, is unclear (e.g. Preece et al., 2014). Regardless, this manifests with the most distal cryptotephra samples trending towards having the highest average SiO_2 values, which is reflected in the Cascade Lake sample (e.g. Davies et al., 2019; Harvey, 2021).

WRAn has a recently updated modelled two-sigma ^{14}C age of 1689–1560 cal yr BP (Reuther et al., 2020). This is slightly younger than previous published estimates (e.g. 1805–1605 cal yr BP, Davies et al., 2016) as the eruption occurred at a time when there is a fluctuation in the ^{14}C calibration curve. An increased number of constraining ages can therefore adjust the most likely modelled age. At Cascade Lake, this age is younger than the radiometric age-model estimate for this depth by ~1370–2170 years (Table S5).

3.1.5 CL-37 (OP tephra)

CL-37 is the second largest pre-19th century peak, with 28 shards/gram. Shards are typically vesicular or cuspate and often have microlite inclusions. This rhyolitic glass population is distinctive from published analyses of glass from Alaska, with notably low wt.% FeO_t (average 0.60%) and CaO (average 0.77%). This characteristic geochemical signature has been observed in some volcanic glasses from Kamchatka (e.g. Portnyagin et al., 2020). CL-37 is shown here to correlate with the Late Holocene caldera forming eruption of Opala (OP), Kamchatka (Andrews et al., 2018; Braitseva et al., 1995, 1997; Kyle et al., 2011; Melekestsev et al., 1992; Plunkett et al., 2015). CL-37 is the first ultra-distal correlation of glass from this eruption outside of Kamchatka.

Here we report an updated modelled eruption age for OP of 1395–1305 cal yr BP (Fig. S4). This was produced using the Tau_Boundary function in OxCal v4.4 with IntCal20

Deleted: (Davies et al., 2019)

Deleted: -

Deleted: -

Deleted: as the new ages and modelling methods reported by Reuther et al. (2020) better constrain the eruption, which occurred at a time when there is a fluctuation in the ^{14}C calibration curve. This age is in good agreement with Steen et al.'s (this volume) PSV-1 age estimate for this depth (Table 4). …

Deleted: This rhyolite

Deleted: (e.g.,

Deleted: -

Deleted: S2

following the methodology of Davies et al. (2016) with ^{14}C ages reported in Braitseva et al. (1995) (Table S4). This is in good agreement with previous published ages for the eruption but is younger than the radiometric age-model estimate for this depth by ~1470–1950 years (Table S5).

3.2 Multimodal/mixed glass populations

Glass shards from six of the remaining analysed shard peaks have mixed or multimodal geochemical data and two have scattered results with no discernible trend. It should be noted here that there are many recorded examples of heterogenous melts with bimodal geochemical trends from Alaska volcanoes (e.g. Aniakchak CFE II, Novarupta-Katmai 1912, see Table S2). However, none of the multi-model samples reported here are interpreted in this way as the different populations do not follow any geochemical trends that would be expected if they were from the same eruption. Instead they form distinct geochemical populations that more likely represent multiple eruptions from different sources.

Higher levels of background shards are present from 35 cm to the surface, and the geochemical 'noise' is also particularly evident in the youngest samples, with all peaks analysed in the past millennium showing either multimodal (>five glass geochemical populations) or scattered data. Detailed geochemical biplots for multimodal sample populations, including those with only a few shards (e.g., CL-0, -2, -31, -61), are shown in Fig. S5. Glass shards from these samples display a mix of morphologies (including platy, cuspate, vesicular and microlitic), which are all commonly seen in tephra in this area. Their grain sizes do not show any differentiation between types (as also seen for the unimodal samples discussed above); these data cannot therefore be used to identify any differences between sub-populations of these samples.

CL-61 is the only analysed mixed sample that pre-dates the past millennium, located between the Ruppert (CL-74, 2800–2130 cal yr BP) and WRAn (CL-48, 1689–1560 cal yr BP) tephras. It has a final age-depth model estimated age of 2450–1700 cal yr BP (2 sigma; Table S6). It contains a few shards that are similar to the rhyodacite from Aniakchak volcano and also an Augustine tephra (Fortin et al., 2019; Waitt and Begét, 2009), but while these volcanoes have known activity at this time (e.g. Bacon et al., 2014; Waitt and Begét, 2009) there are not enough analyses available for a confident correlation.

Deleted: (Braitseva et al., 1995) (Table S4). This is in good agreement with previous published ages for the eruption and with Steen et al.'s (this volume) PSV-1 age estimate for this depth (Table 4)

Deleted: -frequency

Deleted: or scattered data. Geochemical biplots for samples with multiple populations of only a few shards (CL-0, -2, -31, -61) are shown in full in Fig. S3…

Deleted: -

Deleted: -

Deleted: definite

Of the six mixed samples, only two – CL-4 (180-60 cal yr BP, 2 sigma, Table S6) and CL-7 (625-75 cal yr BP, 2 sigma, Table S6) – have populations that can be identified as dominant from the analyses presented here. Rhyodacitic and dacitic glass shards from these samples overlap geochemically with reference data for Aniakchak (Davies et al., 2016) and are interpreted as strong evidence of eruptive activity at Aniakchak, given both the number of shards and the proportion of analyses that they represent. CL-7 also has six points that are geochemically similar to an Early Holocene eruption, KO (~8410–8455 cal yr BP; Braitseva et al., 1997) from Kamchatka, but this does not correlate to any known eruptions from Kamchatka in the timeframe of this deposit. While these are the three most coherent geochemical populations observed in these mixed samples, they are not deemed useful here for chronostratigraphic applications (discussed further in Sect. 5.1.1).

An alternative approach for considering these mixed data is to parse by geochemical trend that can be broadly related to a source rather than to any individual eruption. Given the high levels of background shards it is possible that the chosen shard concentration peaks do not relate directly to primary tephra-fall. This is particularly likely where multiple eruptive events are closely spaced in time and therefore overlap within the temporal resolution of 1 cm of sediment accumulation. As each sample might contain shards from multiple eruptions these data can be seen as recording eruptive activity in a broader period, instead of discrete eruptions or accurately dated events.

Using this source-based classification, it is possible to identify eight geochemical groups, illustrated in Fig. 4, for the four mixed samples from the past ~1000 years, CL-31 and CL-61. Five of these eight geochemical groups correlate with reference glass data for volcanic sources in Alaska (Aniakchak, Mt. Churchill, Redoubt Volcano, Augustine Volcano, Mt. Katmai). These volcanoes all have known eruptions or suspected eruptive activity during this time period (e.g. Cameron et al., 2020).

Figure 4: Geochemical biplots showing mixed-glass samples from Cascade Lake. Bounding shapes represent simplified geochemical fields for potential source volcanoes (to aid visualisation). For the full glass geochemical-data ranges associated with these volcanic sources see Bolton et al. (2020), Davies et al. (2016), Fortin et al. (2019), Zander et al. (2018). Three populations with unknown sources are also shown using the same bounding line and fill. All single point analysis data are listed in Table S2.

Deleted: -
Deleted: by
Deleted: sample
Deleted: six
Deleted: .
Deleted: , Novarupta-
Deleted: over
Deleted: (Alaska Volcano Observatory, 2016)
Formatted: Font: 9 pt
Formatted: Caption
Deleted: , e.g.,,
Deleted: S1

Fig. 4

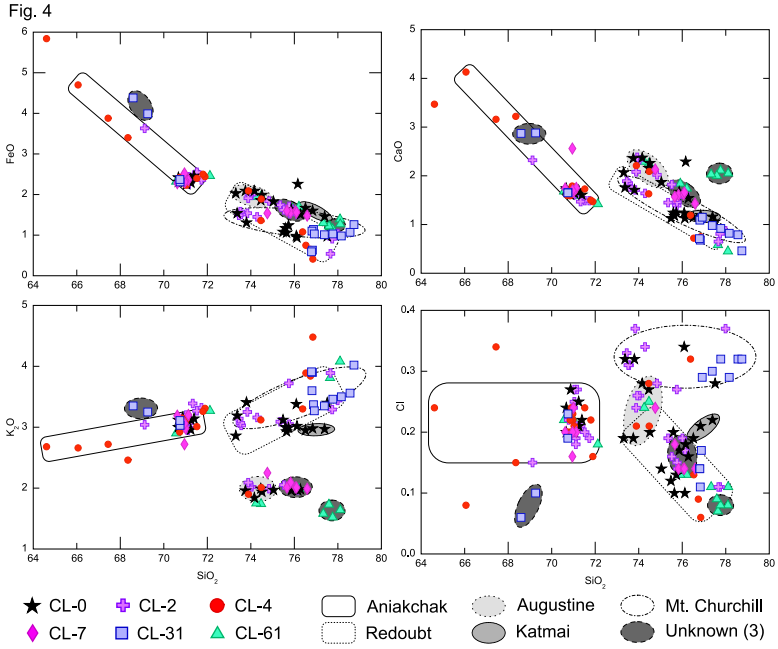

875

4 Bayesian age modelling

Step one of our chronometer comparison (see Sect. 2.3) considered if the individual ages fit their expected stratigraphic order. Steen (2016) noted that two ^{14}C ages from the full core sequence (5.5–7.5 cm and 245–248 cm) were anomalously old compared to their 880 surrounding ages and these were therefore excluded from further consideration. While the ^{210}Pb ages are not discussed here in detail (given their limited applicability to the Late Holocene record) they overlap with the youngest ^{14}C age (2.6–4.5 cm). They therefore help constrain the broad age range (295–60 cal yr BP) of this sample that sits on a plateau in the radiocarbon calibration curve.

885 For step two of our comparison, an overlay of the individually modelled chronometers shows that there are substantial offsets between three of the five ^{14}C ages from this portion of the core and the four available cryptotephra correlated ages (Fig. 5). We place a high level of confidence on these tephra correlated ages as the four identified tephra are well characterised, widely identified in other depositional records (both intra- and extra-regionally), and in a

Deleted: 4
Deleted: et al. (this volume
Deleted: -
Deleted: -
Deleted: out of sequence as they are
Deleted: . They

logical stratigraphic context to one another. The radiometric model also had very low agreement (Amodel=10.3; individual age AI values range from 19.7–78.8), indicating a likely issue within the dataset. Hence, two further ^{14}C ages (30.5–32.5 cm, 85.75–87.75 cm) are also identified as anomalously old and removed here as outliers. Given the trend in the correlated tephra age-model, the lower 138–140 cm ^{14}C age may also be slightly old (unless, for example, there is an unexpected change in sedimentation rates in this part of the core). However, as there are no tephra correlated ages within 30 cm of this ^{14}C sample this could not be confirmed at this stage.

Fig. 5

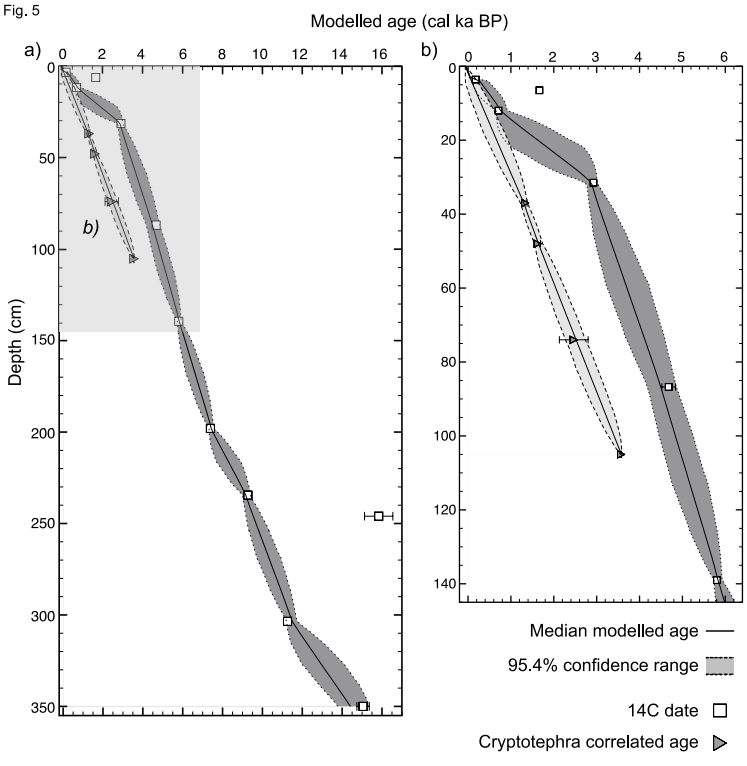

Figure 5: Cascade Lake core CASC-4A/2D multi-method chronometer comparison of downcore age models based on radiocarbon ages (dark grey shading) and correlated tephra ages (data are reported in Table S5). 2 sigma uncertainties are plotted for all samples; where bars are not visible the uncertainty is smaller than the symbol. a) All ^{14}C dates produced by Steen (2016) from CASC-4A/2D; b) the focused upper section with new cryptotephra analyses from this study.

Deleted: PSV-1 tie-points (light grey shading) and

Deleted: (values in Table S3). Correlated tephra ages are overlain at their identified depths and show good agreement with the PSV-1 model. (**a**) Whole model down to 520 cm. Note disagreement between the geomagnetic field model and Burial Lake tie-points from 284-177 cm. PSV-1 model is extrapolated from 520-509 cm (from the base of the unit to the lowest dated sample); (**b**) enlarged 145 cm section, highlighted with the grey shaded box in panel a, showing cryptotephra correlated ages and the substantial offsets between ^{14}C and PSV-1 age models.

For step two of our comparison, an initial overlay of the individually modelled chronometers (Fig. 5) showed that there are substantial offsets between ^{14}C and PSV-1 models above 175 cm, as noted by Steen et al. (this volume). As outlined in Sect. 3.1 and Table 4, the four available cryptotephra correlated ages agree well with PSV-1 tie-points (Fig. 5b) and three further ^{14}C ages (32.5-30.5 cm, 87.75-85.75 cm and 140-138 cm) are therefore also removed as outliers. From 180-290 cm there is also a noticeable divergence between the PSV data model tie-points used from geomagnetic field models and the Burial Lake record (Fig. 5a).

For step three of the comparison, a P_Sequence model was produced (OxCal v4.4., Bronk Ramsey 2009a) that incorporates the remaining data. As Steen (2016) demonstrated better agreement between their chronometers below 2 m depth, ^{14}C ages for the rest of the sequence (down to 3.51 m; Table 1, Figure 2a) are also included here. The data initially included in the model were: six ^{210}Pb ages, four tephra correlated ages and seven ^{14}C ages. For this step, both OxCal's agreement indices and a general student's t-test were used to statistically identify outliers. The initial combined P_Sequence model had good model agreement (Amodel = 81.5) and no further ^{14}C dates were identified as outliers by the student's t-test. The two oldest ^{14}C dates (303–304 cm, 348.5–351 cm) have posterior values that are slightly over the set threshold (9 and 6 respectively compared to the prior of 5) but are not excluded here.

A final model for CASC-4A/2D is shown in Fig. 6. Below the top 4 cm, six ages (four correlated tephra, two ^{14}C) are used to date down to 1.4m (~6 ka BP), providing a robust age model for this portion of the lake sediments. Four ^{14}C ages are used for 1.4–3.51m (~9 ka, 6-15 ka BP) of the sequence and as there are no independent tephra data for this section, these data are reported as provisional. Additional data – especially from independent chronometers - would increase confidence in the lower half of this model.

Deleted: composite

Deleted: using the PSV-1 tie-point ages,

Deleted: cryptotephra

Deleted: the six remaining ^{14}C ages (details for OxCal input are given in File S1). This age-depth model was run with a Student's…

Deleted: outlier

Deleted: , which

Deleted: four ages with strong likelihoods of being outliers (

Deleted: of 68-100;

Deleted: S4). These include two further ^{14}C

Deleted: 199-197 cm and 235.5-233.5 cm) and

Deleted: PSV tie-points from Burial Lake (177 cm and 228 cm). The 284 cm composite depth tie-point from Burial Lake was also removed as it failed the chi-squared test when combined with the tie-point from the pfm9k1b field model and was significantly older than the model results for that depth. These five…

Deleted: not included in the final version of the age-depth model presented here, as their removal improved the model agreement and reduced the associated uncertainties (Fig. S5).…

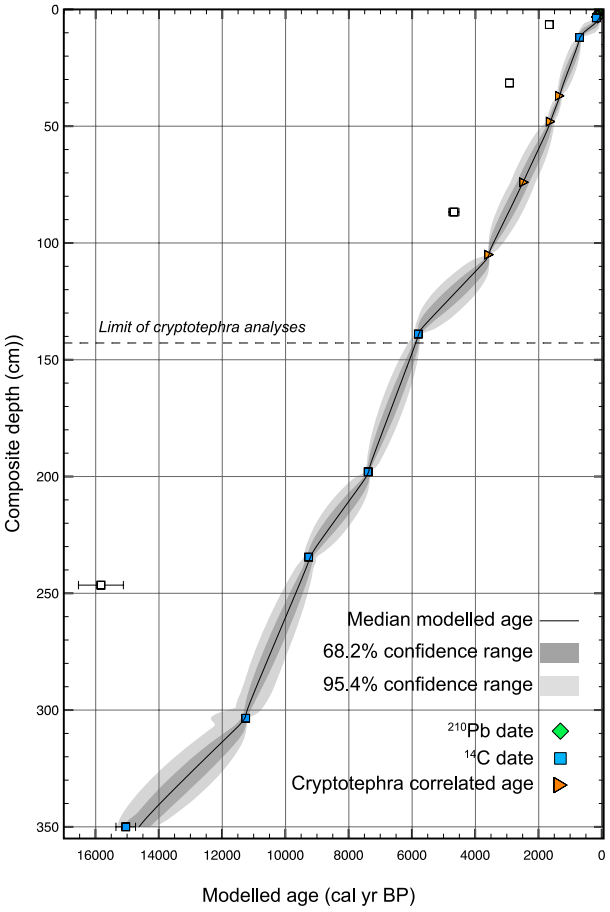

965 **Figure 6:** Age-depth plot showing the final Bayesian age model for Cascade Lake composite core CASC-4A/2D. Shaded areas show the 1 sigma (68.2%) and 2 sigma (95.4%) confidence ranges. Filled symbols are included in the model and white symbols are identified as outliers. 2 sigma errors are included for all ages; where they are not visible the error is smaller than the symbol used. Full details and values can be found in Table S6.

5 Discussion

The data reported here have implications for cryptotephra records in northwestern North America and for Arctic sedimentary sequences and age models through the successful application of multi-chronometer Bayesian age-modelling.

5.1 Cryptotephra in Arctic Alaska

This study demonstrates that identifiable concentrations of volcanic glass reach the north flank of the Brooks Range and can be used as chronostratigraphic tools where clear evidence of primary tephra-fall is preserved. In particular, this is the first report of ultra-distal glass from the Late Holocene eruption of Opala, Kamchatka (>3000 km from Cascade Lake), as well as an unknown tephra, CL-96, likely from a source in the Alaska Peninsula-Aleutian Arc. Ruppert tephra and Aniakchak CFE II are both documented on the southern slope of the Brooks Range (Monteath et al., 2017), and their distributions are expanded here across this large topographic barrier. This is also the first distal identification of WRAn this far to the northwest of Mt. Churchill.

Glass shard morphologies and preliminary grain size measurement data are reported for the unimodal tephra populations at Cascade Lake. However, these data are not used here to differentiate between samples or subpopulations – for example, the five tephra with distinct geochemical populations all have similar maximum axis length and sphericity values. This is not surprising for maximum axis length, as previous studies have shown that the grain sizes reported here (20-40 μm) are commonly found in deposits located 500–3000 km from their source (Stevenson et al., 2015). Quantitative grain size measurements provide valuable information for a range of research questions but are not commonly reported for cryptotephra (Saxby et al., 2020). Hence, these data are provided here as preliminary values for distal deposits of these correlated tephra.

While the cryptotephra profile here only covers the Late Holocene, it highlights eruptive events that are both locally important and widespread and provides possibilities for correlating proxy data within North America and across the Pacific in Kamchatka. Our focus was specifically on the past ~4 ka as there are several widespread, well-dated and geochemically characterised tephra within Alaska during this time period. From 12–4 ka, there is a paucity of well-dated regional tephra that are documented and fully characterised,

Formatted: Normal

Deleted: S3.

Deleted: ,

Deleted: or

Deleted: -

but it is possible that new tephra from other regions may be identified as more tephra studies are published, as seen here with OP.

Compared to the cryptotephra stratigraphies published in Monteath et al. (2017) from Ruppert Lake and Woody Bog Pond, located ~150 km south of Cascade Lake on the southern slope of the Brooks Range, large differences can be seen in both the number of primary tephra preserved and the overall shard presence and concentrations. Reported glass abundances at the southern sites are at least an order of magnitude higher than those from Cascade Lake (100s–1000s vs 10s shards/gram or less). This likely relates in part to the topographic barrier presented by the Brooks Range, causing increased rain-out of shards being transported from the south (e.g. in north trending plumes from Aniakchak CFE II) and deposition of shards before they reach the northern slope (e.g. Watt et al., 2015). Other factors may include lake size and bathymetry, catchment size, local topography and hydrology (e.g. Pyne-O'Donnell, 2010). Cascade Lake is an order of magnitude larger and deeper than the southern sites and hence has a larger surface area (~1 km^2 vs 0.04 and 0.01 km^2) but its catchment area is not proportionally larger (~10 km^2 vs <4 km^2) and it has no current inflow. Hence, it is suggested here that topography is a primary influence on Cascade Lake shard concentrations (compared to other sites further south) and not lake characteristics.

There are common issues affecting cryptotephra research in Alaska that still apply at this distal, Arctic site. Cascade Lake is downwind of multiple active volcanic sources where records show that multiple closely spaced eruptions have occurred. This, combined with relatively low sediment accumulation rates, is likely to cause geochemical variability within individual samples where 1 cm of sediment represents decades of accumulation (25-67 years/cm calculated for Cascade Lake's 15 ka age-depth model). The presence of glass in ~75% of the samples analysed here shows a level of background deposition that must be considered when interpreting data from identified shard concentration peaks. This is particularly important here as a) the peak concentrations are relatively low compared to other cryptotephra records in the region (e.g. Davies, 2018; Monteath et al., 2017; Payne and Blackford, 2004), and b) the signal:noise ratio between peaks that have been correlated with known eruptions and the (fairly consistent) background shard concentration is relatively high. Reworking and secondary deposition of tephra in the landscape can also be a substantial issue

Deleted: , as

Deleted: –

Deleted: . Other factors may include lake size and bathymetry, catchment size, local topography and hydrology….

for records from this region, but this is not a likely problem at Cascade Lake as there is so little tephra present in the area (i.e. there is no clear source for tephra to be reworked from).

Furthermore, a broader issue that affects how much confidence can be attributed to a geochemical correlation is the available glass data for reference material from given eruptions or volcanoes. Here, this is relatively limited in scope compared to the number of Late Holocene eruptions reported in Alaska. Comparisons are often made with tephra data that relate to a small number of eruptions (or possibly only one) from a subset of the volcanoes with known activity. A degree of uncertainty will therefore affect correlations with given eruptions or sources until more characterisations are published from both proximal and distal tephra deposits.

Deleted: The shard concentration profile reported for Cascade Lake is affected by closely spaced eruptions from multiple sources combined with relatively low sediment accumulation rates, causing geochemically variability within individual samples. The presence of glass in the majority of samples analysed shows a level of background deposition that must be considered when interpreting data from identified shard concentration peaks. This is particularly important here as the signal:noise ratio between the peaks that have been correlated with known eruptions and the (fairly consistent) background shard concentration is relatively high. This is mostly due to the low concentrations of shards in the identified peaks, compared to other cryptotephra records in the area. …

5.1.1 Multi-modal samples and historical activity

The issue of 'clear evidence of primary tephra-fall' being preserved is one that affects all cryptotephra records. Low numbers of shard analyses cannot be interpreted as conclusive evidence of an eruption, especially if multiple geochemical populations or trends are observed. This appears to only be a problem for certain parts of the Cascade Lake tephrostratigraphic record; there are discernible changes in shard concentrations and sample compositions from the younger portion of the core. For example, samples analysed from 0–30 cm have multiple geochemical populations, which are not frequently seen below this. This is likely related to an overall increase in the shard-concentrations and peak density that is particularly notable for the top 15 cm of the core. These differences could be the result of a myriad of regional (e.g. weather patterns) and local (e.g. reworking) factors that affect the distribution and preservation of shards (e.g. Watson et al., 2015), but at Cascade Lake we hypothesize this may largely be the result of changing sedimentation rates.

Overall, it is possible that the background shards evident in the full Cascade Lake shard concentration profile (Fig. 2b) could be the result of taphonomic problems such as reworking, bioturbation or secondary in-wash. However, this is not likely a substantial problem for the record presented here. The lake sediments are laminated and do not show signs of deformation (from either in-situ processes or the core extraction). These shards are also unlikely to represent significant reworking from the surrounding landscape, or within the lake sediment itself, as there is little ash in the area and therefore no obvious source for

Deleted: samples

Deleted: contains multiple geochemical populations/trends.

Deleted: -0

Deleted: However, this view may be biased by the relatively higher number of samples with more than five analyses in this period. Also, the overall

Deleted: concentration profile over

Deleted: has higher average and peak shard concentration values than the rest of the analysed sediment.…

Deleted: eruption style, plume altitude, wind direction and strength, shard characteristics) and local (e.g.

Deleted: fallout on snow, sediment accumulation, hydrology, bioturbation) factors that affect the

Deleted: , deposition, reworking,

Deleted: ultimately

Deleted: . A succinct summary for these factors relating to cryptotephra in peatlands is given in Watson et al., (2015), and is …

Deleted: applicable for

redeposition. Furthermore, the tails and multiple peaks do not show repetition of a common geochemical signal, which would be expected if the shards were reworked or secondary in-wash (e.g., as seen with Askja 1875 in Swedish lake in Davies et al., 2007, or with the eastern lobe of the White River Ash at Sydney Bog in Jensen et al., 2021).

Geochemical data from the top 30 cm do show some repetition between samples so it is not possible to rule out reworking for this portion of the core, but this may also be the result of multiple eruptions from single sources in this ~1000-year time period. Sedimentation rates are relatively low at this site, particularly for this interval at 30–67 years/cm (Table S6), which would cause increased overlap for closely spaced events. Hence, the glass shard data from the last ~1000 years are interpreted as evidence for trace amounts of tephra reaching the north flank of the Brooks Range. Beyond the five clearly defined cryptotephra samples described above, we present evidence of volcanic activity from Augustine, Redoubt, Aniakchak, Mt. Churchill, Mt. Katmai (e.g., Bolton et al., 2020) and further possible sources in Kamchatka and Alaska based on geochemically similarities to available reference data for characterised eruptions (Fig. 4). This supposition is supported by records of eruptions from the past millennium (e.g., Cameron et al., 2020), which include Novarupta-Katmai 1912, six eruptions from Redoubt and 14 from Augustine. A higher sampling resolution for this period may help distinguish individual eruptive events and resolve this question, but with such low sedimentation rates it may instead highlight the limit of this record's preservation potential.

Eruptions in the past millennium from both Mt. Churchill and Aniakchak have been identified distally elsewhere in Alaska. For Mt. Churchill there is published evidence for an eruption in the last 500 years: the Lena tephra is dated to 310–285 cal yr BP (Payne et al., 2008). It is possible that shards from CL-0 and -2 relate to this tephra, but their modelled age is too young to support a correlation (AD 1930-2010). Proximal records at Aniakchak indicate multiple eruptions have occurred between 560 to 70 yr BP (Bacon et al., 2014; Neal et al., 2001), and a distal tephra in the Akhlun Mountains, southwest Alaska is dated at around 400 yr BP (Kaufman et al., 2012). The large number of analyses that geochemically correlate with Aniakchak (47, including 4 dacitic points) over four samples from Cascade Lake (CL-0, 2, 4 and 7) are interpreted here as representing at least one eruptive event in the last ~400 years. However, any correlations here are limited by both the lack of glass

Deleted: .

Deleted: Beyond the five clearly defined cryptotephra samples, we present evidence here of volcanic activity using glass that is geochemically similar to reference data for Mt. Augustine, Redoubt, Aniakchak, Mt. Churchill, Novarupta-Katmai (e.g. Bolton et al., 2020) and further possible sources in Kamchatka and Alaska. Focusing on the modern period, this is interpreted as evidence for trace amounts of glass reaching the north flank of the Brooks Range from known eruptions, but without the resolution to interpret individual eruptive events. These shards are unlikely to represent significant reworking from the surrounding landscape, or within the lake sediment itself, as there is little ash in the area. This supposition is supported by the record of known eruptions in the past millennium, including Novarupta-Katmai 1912, six eruptions from Redoubt and 13 from Augustine (Alaska Volcano Observatory, 2016). ¶ Furthermore, sedimentation rates calculated from the age-model data using OxCal v4.4 (Table S3) show that there is a significant decrease, by ~50%, for the depth interval of 12-4 cm (~1840-1250 CE) compared to the Holocene average values (0.015 vs 0.029 cm a^{-1}). This period, coinciding with the Little Ice Age, is therefore expected to show increased background shard concentrations and multi-modal data from 1-cm-resolution samples as each centimetre represents ~67 years of accumulation compared to ~25-40 years as seen here over the Holocene. A higher resolution record for this time period may help to address some of the issues detailed here.¶ For Mt.

Deleted: -

Deleted: It forms a visible bed in Yukon Territory (Preece et al., 2014) where it sits on top of ~10 cm of peat accumulation above the WRAe. It is possible that shards from CL-0 and -2 relate to these events, although their age is younger than expected. There has not been any observed modern eruptive activity at Mt. Churchill. ¶ There is published evidence for proximal activity at Aniakchak

Deleted: (Neal et al., 2001), but only a small proportion of the associated whole rock geochemical data have a rhyodacitic composition similar to the mid-Holocene CFE II eruption (Bacon et al., 2014). Distal tephra preserved in sediment from lakes in the Akhlun Mountains, southwest Alaska, however, have similar glass geochemistry and have been da

Deleted: . As our age model places the Cascade Lake samples between 350-100 cal yr BP, this currently precludes correlation with these known events. This age range is associated with a relatively high uncertainty due to decreased sedimentation rates, so it is possible the chronology does not negate these correlations, but an alternative correlation with a younger eruption from Aniakchak (that has not yet been identified distally) cannot be ruled out.…

Deleted: therefore

Deleted: as

Deleted: from Aniakchak

geochemical data on proximal tephra and the high uncertainty in modelled ages for these samples at Cascade Lake. Our age model places these samples between 630–10 cal yr BP (2-sigma) due to decreased sedimentation rates at this time, so additional correlation(s) with other younger eruption(s) from Aniakchak also cannot be ruled out.

5.2 Cascade Lake age models

It is not uncommon for ages produced by multiple chronometers to diverge over part or all of a sediment sequence. Individual chronometers have their own inherent strengths and weaknesses, and their different physical properties can be affected by a number of different processes, which in turn affect the preserved and eventually measured signal (e.g. Davies et al., 2018). This is somewhat disheartening as using multiple techniques should provide a check for bias and inaccurate data, but additional independent data can be used to identify and reconcile observed offsets, as shown here.

Once any obvious outliers have been addressed (i.e. step one from Sect. 2.3), it is not always easy to resolve any remaining disagreements between chronometers. Here, the importance of independent chronological validation from marker horizons (Late Holocene cryptotephra, which provide additional data in a key period), and the power of Bayesian statistics for age modelling are demonstrated. The identification of periods of offset and anomalous or biased ages can allow further investigation of the potential causes, such as mechanical (e.g. mobilisation or redeposition) or chemical (e.g. alteration or degradation) processes affecting the analysed sample material. In this case, however, the resulting age-depth model for the whole core can still be strengthened by the addition of further independent chronological data, especially for the lower section (1.42–3.51 m).

The commonly applied method of ^{14}C dating can have low reported uncertainties, but is restricted at some Arctic sites by a lack of suitable material. Where macrofossils are available, they may be affected by old carbon contamination or the redeposition of older material. Cascade Lake's location in limestone terrain likely resulted in a hard-water effect, which could explain the anomalously old ^{14}C ages identified here; four of the Holocene ^{14}C ages are variably 500–5000 years too old compared to median modelled ages for their given depths. As mentioned in other studies the use of either terrestrial material or the humic fraction of sediment is recommended, especially when in limestone terrane (Lowe and

Deleted: steps

Deleted: and two

Deleted: 4

Deleted: For example, from 303-175 cm in Cascade Lake cores there is a divergence between PSV-1 tie-points from geomagnetic field models, from Burial Lake and ^{14}C ages. Logically, the geomagnetic field models incorporate data from multiple regional palaeomagnetic records, which should give a valuable, albeit spatially smoothed, resulting record for the area. Their reliability at any given coordinate, however, will depend on the amount and quality of data that is in close proximity. A single, nearby well-dated PSV record (here, Burial Lake) could arguably be more relevant than a field model that incorporates multiple datasets. The use of terrestrial macrofossils for radiocarbon dating at Burial Lake and their consistency over the sedimentary sequence suggests they are not affected by, for example, old carbon effects. But, if accurate, the Burial Lake tie-point ages are up to 2000 years older than the other methods for the same composite depths. Outlier analysis performed within OxCal v4.4 was used to assess the ages and statistically identify remaining outliers here (two ^{14}C ages and three Burial Lake PSV tie-points) in order to resolve this divergence.¶
The combination of all three chronometers using Bayesian modelling techniques is therefore shown to result in a refined dataset that produces a reliable age model for the past ~21 ka. This

Deleted: – here,

Deleted: –

Deleted: . Furthermore, the

Deleted: Data from Cascade Lake show that PSV-1 provides reliable and accurate tie-points in the Late Holocene that are in agreement with four cryptotephra correlated ages. Comparison of these data across the whole core shows that at least six ^{14}C ages are too old, including two initially identified as out of sequence (likely old carbon contamination). However, while the 'best ages' produced by PSV-1 are in good agreement with the final age-depth model, the associated uncertainty produced by the geomagnetic field models (± 500 years) is broad compared to other methods that can be applied to this time period.¶

Deleted: more

Deleted: lower associated errors

Deleted: shown by

Deleted: reported

Deleted: . Only

Deleted: eleven analysed samples were included in the final age-depth model and the identified outliers were…

Deleted: -

Walker, 2000). Nonetheless, this study adds to a growing body of literature that demonstrates that using multiple independent chronometers with Bayesian age modelling techniques can produce accurate and reliable age-depth models for Arctic lake sediments.

6 Conclusions

This research demonstrates the potential for dating Arctic lake sediments in Alaska using cryptotephra correlations. The advantages of tephrochronology include the relatively long period of time over which it can be applied (compared to ^{210}Pb and ^{14}C), the level of precision associated with known tephra ages (especially those from documented historical events) and the potential for independently testing and validating other chronometers with tephra correlated ages. We suggest here that the most robust age models can be produced by using a combination of chronostratigraphic techniques in a Bayesian statistical model. While cryptotephra are best defined regionally for the Late Holocene, it is possible that other well-dated cryptotephra from Alaska (e.g. the Early Holocene caldera forming eruptions from Fisher, Stelling et al., 2005; the late Pleistocene Tephra D, Davies et al., 2016) and ultra-distal sources (e.g. Kamchatka, Japan) could be identified in northern regions.

Deleted: PSV tie-points and

Deleted: longer

Deleted: ,

Deleted: and their

Data availability

The major element glass geochemistry data and associated metadata for individual tephra grains will be made available publicly though the Alaska Volcano Observatory Geochemical Database (Cameron et al., 2019; http://avo.alaska.edu/geochem), part of the larger Geologic Database of Information on Volcanoes in Alaska (GeoDIVA). The Bayesian age-depth models generated in this study, including the underlying radiometric ages are available as supplementary data.

Deleted: model

Deleted: radiocarbon

Deleted: , lead ages and palaeomagnetic secular variation data

Deleted: supplements to both this paper and Steen et al. (this volume).…

Supplement information

File S1: OxCal age-depth model input.

Figure S1: Cascade Lake core images, lithological units, wet bulk density (WBD), organic matter (OM) and biogenic silica (BSi) data from Steen (2016).

Figure S2: Optical microscopy glass shard images for the five unimodal cryptotephra populations reported from Cascade Lake.

Figure S3: Bayesian Tau_Boundary probability density function plots derived using OxCal v4.4 and IntCal20 for the age of Aniakchak CFE II tephra with: all ^{14}C dates are included (grey right-hand distribution); two ^{14}C dates removed (green central distribution); and all but two ^{14}C dates and the NGRIP ice core chronology age (Pearce et al., 2017) (blue left-hand bar). See Table S4 for the ages used for this model.

Figure S4: Bayesian Tau_Boundary probability density function plots derived using OxCal v4.4 and IntCal20 for the age of OP tephra, Opala, Kamchatka. See Table S4 for the ages used for this model.

Figure S5: Major element glass geochemical biplots showing wt.% SiO_2 vs K_2O and FeO vs CaO for samples with multiple geochemical populations. (**a**) CL-0 and CL-2; (**b**) CL-4 and CL-7; (**c**) CL-31 and CL-61; (**d**) CL-0, -2, -4 and -7 plotted both by sample and by geochemical correlation with a source volcano or region.

Figure S6: OxCal age-depth output for the final Bayesian model for Cascade Lake. The students'-t outlier analysis results shown good agreement.

Table S1: Grain size measurements for unimodal tephra samples reported at Cascade Lake. Measurements were made using optical microscopy (Grain depth) and image analysis with ImageJ software. Geometric size (here, d_ψ – diameter of a volume equivalent sphere) and sphericity (ψ) were calculated following the methods reported in Saxby et al. (2020).

Table S2: Single point major element glass geochemical data for Cascade Lake samples and reference material.

Table S3: Secondary standard data (ID 3506 and Old Crow) for EPMA glass analyses of Cascade Lake samples and reference material.

Table S4: Ages for tephras reviewed within this study, listed by associated tephra.

Table S5: OxCal age model output for the initial multi-method chronometer comparison. Age models based on a) radiometric ages and b) correlated tephra ages.

Table S6: Final OxCal age model output for 0-3.51 m of CASC13-4A/2D, Cascade Lake.

Deleted: Figure S1

Deleted: S2

Deleted: S3

Deleted: S4: OxCal age-depth plot output for the initial Bayesian model for Cascade Lake (v1). Students'-t outlier analysis results are shown. Four ages have more than 50% chance of being an outlier. BL-284 is also excluded as it has an outlier posterior value of 49 and it fails the chi^2 when combined with pfm9k1b-284. ¶
Figure S5

Deleted: (v2). Five outliers from the previous model (v1) were removed and the…

Deleted: Table S1

Deleted: S2

Deleted: Table S3: Final OxCal age model output for 0-520 cm of CASC13-4A/2D, Cascade Lake.¶

Author contribution

LJD carried out the research, helped conceptualise the study, and wrote the manuscript. DSK and BJLJ helped conceptualise and fund the study and revised the manuscript. DSK provided the samples. BJLJ carried out some of the analyses.

Competing interests

The authors declare that they have no conflict of interest.

Acknowledgements

Many thanks to everyone who has been involved in producing the data discussed within this paper. Jason Briner, David Fortin and Liz Ceperley helped core Cascade Lake; LacCore staff assisted with the initial core analysis and curation. Flett Research, Ltd. provided the ^{210}Pb measurements and the W.M. Keck Carbon Cycle Accelerator Mass Spectrometry Laboratory at UC Irvine provided the ^{14}C measurements. Vera Ponomareva

discussed and plotted reference data for an initial comparison with Kamchatkan tephra data. Ben Andrews supplied reference material from Opala tephra that were analysed at the University of Alberta. Josephine Bailey assisted with image analysis methodologies and grain size calculations.

Funding sources

Initial research was funded by a National Science Foundation grant (#1107662, DSK). Subsequent work at the University of Alberta was funded by the Natural Sciences and Engineering Research Council of Canada Discovery Grant and Accelerator Grant (NSERC Discovery grant: #RGPIN-2018-04926; Accelerator: #RGPAS-2018-52250; both BJLJ). LJD would like to recognise support from the Leverhulme Trust through an Early Career Fellowship since October 2020.

References

Abbott, M. B. and Stafford, T. W.: Radiocarbon Geochemistry of Modern and Ancient Arctic Lake Systems, Baffin Island, Canada, Quat. Res., 45(3), 300–311, doi:10.1006/qres.1996.0031, 1996.

Adolphi, F. and Muscheler, R.: Synchronizing the Greenland ice core and radiocarbon timescales over the Holocene-Bayesian wiggle-matching of cosmogenic radionuclide records, Clim. Past, 12(1), 15–30, doi:10.5194/cp-12-15-2016, 2016.

Ager, T. A.: Late Quaternary vegetation and climate history of the central Bering land bridge from St. Michael Island, western Alaska, Quat. Res., 60(1), 19–32, doi:10.1016/S0033-5894(03)00068-1, 2003.

Alaska Volcano Observatory: Alaska Volcano Observatory Online Library, [online] Available from: https://avo.alaska.edu/volcanoes/index.php, 2016.

Andrews, B. J., Dufek, J. and Ponomareva, V.: Eruption dynamics and explosive-effusive transitions during the 1400 cal BP eruption of Opala volcano, Kamchatka, Russia, J. Volcanol. Geotherm. Res., 356, 316–330, doi:10.1016/j.jvolgeores.2018.02.019, 2018.

Bacon, C. R., Neal, C. A., Miller, T. P., McGimsey, R. G. and Nye, C. J.: Postglacial eruptive history, geochemistry, and recent seismicity of Aniakchak volcano, Alaska Peninsula., 2014.

Barletta, F., St-Onge, G., Channell, J. E. T., Rochon, A., Polyak, L. and Darby, D.: High-resolution paleomagnetic secular variation and relative paleointensity records from the western Canadian Arctic: implication for Holocene stratigraphy and geomagnetic field behaviour, Can. J. Earth Sci., 45(11), 1265–1281, doi:10.1139/E08-039, 2008.

van der Bilt, W. G. M., Lane, C. S. and Bakke, J.: Ultra-distal Kamchatkan ash on Arctic Svalbard: Towards hemispheric cryptotephra correlation, Quat. Sci. Rev., 164, 230–235, doi:10.1016/j.quascirev.2017.04.007,

2017.
Blaauw, M. and Christen, J. A.: Radiocarbon peat chronologies and environmental change, J. R. Stat. Soc. Ser. C Appl. Stat., 54(4), 805–816, doi:10.1111/j.1467-9876.2005.00516.x, 2005.
Blackford, J. J., Payne, R. J., Heggen, M. P., de la Riva Caballero, A. and van der Plicht, J.: Age and impacts of the caldera-forming Aniakchak II eruption in western Alaska, Quat. Res. (United States), 82(1), 85–95, doi:10.1016/j.yqres.2014.04.013, 2014.
Blockley, S. P. E., Pyne-O'Donnell, S. D. F., Lowe, J. J., Matthews, I. P., Stone, A., Pollard, A. M., Turney, C. S. M. and Molyneux, E. G.: A new and less destructive laboratory procedure for the physical separation of distal glass tephra shards from sediments, Quat. Sci. Rev., 24(16–17), 1952–1960, doi:10.1016/j.quascirev.2004.12.008, 2005.
Blockley, S. P. E., Bronk Ramsey, C. and Pyle, D. M.: Improved age modelling and high-precision age estimates of late Quaternary tephras, for accurate palaeoclimate reconstruction, J. Volcanol. Geotherm. Res., 177(1), 251–262, doi:10.1016/j.jvolgeores.2007.10.015, 2007.
Bolton, M., Jensen, B. J. L., Wallace, K. L., Praet, N., Fortin, D., Kaufman, D. S. and De Batist, M.: Machine learning classifiers for attributing tephra to source volcanoes: An evaluation of methods for Alaska tephras, J. Quat. Sci., In-revisio, n.d.
Braitseva, O. A., Melekestsev, I. V., Ponomareva, V. V. and Sulerzhitsky, L. D.: Ages of calderas, large explosive craters and active volcanoes in the Kuril-Kamchatka region, Russia, Bull. Volcanol., 57(6), 383–402, doi:10.1007/BF00300984, 1995.
Braitseva, O. A., Ponomareva, V. V., Sulerzhitsky, L. D., Melekestsev, I. V. and Bailey, J.: Holocene Key-Marker Tephra Layers in Kamchatka, Russia, Quat. Res., 47(2), 125–139, doi:10.1006/qres.1996.1876, 1997.
Brock, F., Lee, S., Housley, R. A. and Bronk Ramsey, C.: Variation in the radiocarbon age of different fractions of peat: A case study from Ahrenshöft, northern Germany, Quat. Geochronol., 6(6), 550–555, doi:10.1016/j.quageo.2011.08.003, 2011.
Bronk Ramsey, C.: Deposition models for chronological records, Quat. Sci. Rev., 27(1–2), 42–60, doi:10.1016/j.quascirev.2007.01.019, 2008.
Bronk Ramsey, C.: Dealing with Outliers and Offsets in Radiocarbon Dating, Radiocarbon, 51(3), 1023–1045, doi:10.1017/S0033822200034093, 2009.
Bronk Ramsey, C.: Recent and Planned Developments of the Program OxCal, Radiocarbon, 55(3–4), 720–730, doi:10.2458/azu_js_rc.55.16215, 2013.
Cameron, C. E., Mulliken, K. M., Crass, S. W., Schaefer, J. R. and Wallace, K. L.: Alaska Volcano Observatory geochemical database, version 2., 2019.
Christen, J. A., Clymo, R. S. and Litton, C. D.: A Bayesian Approach to the Use of 14C Dates in the Estimation of the Age of Peat, Radiocarbon, 37(02), 431–441, doi:10.1017/S0033822200030915, 1995.
Cook, E., Portnyagin, M., Ponomareva, V., Bazanova, L., Svensson, A. and Garbe-Schönberg, D.: First identification of cryptotephra from the Kamchatka Peninsula in a Greenland ice core: Implications of a widespread marker deposit that links Greenland to the Pacific northwest, Quat. Sci. Rev., 181, 200–206,

doi:10.1016/j.quascirev.2017.11.036, 2018.
Coulter, S. E., Pilcher, J. R., Plunkett, G., Baillie, M., Hall, V. A., Steffensen, J. P., Vinther, B. M., Clausen, H. B. and Johnsen, S. J.: Holocene tephras highlight complexity of volcanic signals in Greenland ice cores, J. Geophys. Res. Atmos., 117(21), 1–11, doi:10.1029/2012JD017698, 2012.
Cox, A.: Latitude Dependence of the Angular Dispersion of the Geomagnetic Field, Geophys. J. R. Astron. Soc., 20(3), 253–269, doi:10.1111/j.1365-246X.1970.tb06069.x, 1970.
Davies, L. J.: The development of a Holocene cryptotephra framework in northwestern North America, University of Alberta., 2018.
Davies, L. J., Jensen, B. J. L., Froese, D. G. and Wallace, K. L.: Late Pleistocene and Holocene tephrostratigraphy of interior Alaska and Yukon: Key beds and chronologies over the past 30,000 years, Quat. Sci. Rev., 146, 28–53, doi:10.1016/j.quascirev.2016.05.026, 2016.
Davies, L. J., Appleby, P., Jensen, B. J. L., Magnan, G., Mullan-Boudreau, G., Noernberg, T., Shannon, B., Shotyk, W., van Bellen, S., Zaccone, C. and Froese, D. G.: High-resolution age modelling of peat bogs from northern Alberta, Canada, using pre- and post-bomb 14C, 210Pb and historical cryptotephra, Quat. Geochronol., 47, 138–162, doi:10.1016/j.quageo.2018.04.008, 2018.
Davies, L. J., Jensen, B. J. L. and Locock, A. J.: Do visible Holocene tephra from Mt. Churchill, Alaska, display varying geochemistry across their distributions?, in INQUA XX Congress, Dublin., 2019.
Davies, S. M.: Cryptotephras: The revolution in correlation and precision dating, J. Quat. Sci., 30(2), 114–130, doi:10.1002/jqs.2766, 2015.
Denton, J. S. and Pearce, N. J. G.: Comment on "A synchronized dating of three Greenland ice cores throughout the Holocene" by B. M. Vinther et al.: No Minoan tephra in the 1642 B.C. layer of the GRIP ice core, J. Geophys. Res. Atmos., 113(4), 1–7, doi:10.1029/2007JD008970, 2008.
Deschamps, C. E., St-Onge, G., Montero-Serrano, J. C. and Polyak, L.: Chronostratigraphy and spatial distribution of magnetic sediments in the Chukchi and Beaufort seas since the last deglaciation, Boreas, 47(2), 544–564, doi:10.1111/bor.12296, 2018.
Donadini, F., Korte, M. and Constable, C.: Millennial variations of the geomagnetic field: From data recovery to field reconstruction, Space Sci. Rev., 155(1–4), 219–246, doi:10.1007/s11214-010-9662-y, 2010.
Donovan, J., Kremser, D., Fournelle, J. H. and Goemann, K.: Probe for EPMA: Acquisition, automation and analysis, [online] Available from: www.probesoftware.com, 2015.
Dorfman, J. M.: A 37,000-year Record of Paleomagnetic and Environmental Magnetic Variability from Burial Lake, Arctic Alaska., Oregon State University., 2013.
Fierstein, J.: Explosive eruptive record in the Katmai region, Alaska Peninsula: An overview, Bull. Volcanol., 69(5), 469–509, doi:10.1007/s00445-006-0097-y, 2007.
de Fontaine, C. S., Kaufman, D. S., Scott Anderson, R., Werner, A., Waythomas, C. F. and Brown, T. A.: Late Quaternary distal tephra-fall deposits in lacustrine sediments, Kenai Peninsula, Alaska, Quat. Res., 68(1), 64–78, doi:10.1016/j.yqres.2007.03.006, 2007.
Fortin, D., Praet, N., McKay, N. P., Kaufman, D. S., Jensen, B. J. L., Haeussler, P. J., Buchanan, C. and De

Batist, M.: New approach to assessing age uncertainties – The 2300-year varve chronology from Eklutna Lake, Alaska (USA), Quat. Sci. Rev., 203, 90–101, doi:10.1016/j.quascirev.2018.10.018, 2019.
Gaglioti, B. V., Mann, D. H., Jones, B. M., Pohlman, J. W., Kunz, M. L. and Wooller, M. J.: Radiocarbon age-offsets in an arctic lake reveal the long-term response of permafrost carbon to climate change, J. Geophys. Res. Biogeosciences, 119(8), 1630–1651, doi:10.1002/2014JG002688, 2014.
Global Volcanism Program: Volcanoes of the World, v. 4.8.0., , doi:https://doi.org/10.5479/si.GVP.VOTW4-2013, 2013.
Jensen, B. J. L.: Tephrochronology of middle to late Pleistocene loess in east-central Alaska, University of Alberta, Edmonton, Alberta, Canada, MSc thesis., 2007.
Jensen, B. J. L., Froese, D. G., Preece, S. J., Westgate, J. A. and Stachel, T.: An extensive middle to late Pleistocene tephrochronologic record from east-central Alaska, Quat. Sci. Rev., 27(3–4), 411–427, doi:10.1016/j.quascirev.2007.10.010, 2008.
Jensen, B. J. L., Pyne-O'Donnell, S., Plunkett, G., Froese, D. G., Hughes, P. D. M., Sigl, M., McConnell, J. R., Amesbury, M. J., Blackwell, P. G., van den Bogaard, C., Buck, C. E., Charman, D. J., Clague, J. J., Hall, V. A., Koch, J., Mackay, H., Mallon, G., McColl, L. and Pilcher, J. R.: Transatlantic distribution of the Alaskan White River Ash, Geology, 42(10), 875–878, doi:10.1130/G35945.1, 2014.
Jensen, B. J. L., Beaudoin, A. B., Clynne, M. A., Harvey, J. and Vallance, J. W.: A re-examination of the three most prominent Holocene tephra deposits in western Canada: Bridge River, Mount St. Helens Yn and Mazama, Quat. Int., 500, 83–95, doi:10.1016/j.quaint.2019.03.017, 2019.
Jensen, B. J. L., Davies, L. J., Nolan, C., Pyne-O'Donnell, S. D. F., Monteath, A. J., Ponomareva, V. V., Portnyagin, M. V., Cook, E., Plunkett, G., Booth, R. K., Hughes, P. D. M., Bursik, M., Luo, Y., Cwynar, L. C. and Pearson, D. G.: A latest Pleistocene and Holocene composite tephrostratigraphic framework for paleoenvironmental records for northeastern North America, Quat. Sci. Rev., n.d.
Karrow, P. F. and Anderson, T. W.: Palynological Study of Lake Sediment Profiles from Southwestern New Brunswick: Discussion, Can. J. Earth Sci., 12(10), 1808–1812, doi:10.1139/e75-161, 1975.
Kaufman, D. S., Jensen, B. J. L., Reyes, A. V., Schiff, C. J., Froese, D. G. and Pearce, N. J. G.: Late Quaternary tephrostratigraphy, Ahklun Mountains, SW Alaska, J. Quat. Sci., 27(4), 344–359, doi:10.1002/jqs.1552, 2012.
Kaufman, D. S., Axford, Y. L., Henderson, A. C. G., McKay, N. P., Oswald, W. W., Saenger, C., Anderson, R. S., Bailey, H. L., Clegg, B., Gajewski, K., Hu, F. S., Jones, M. C., Massa, C., Routson, C. C., Werner, A., Wooller, M. J. and Yu, Z.: Holocene climate changes in eastern Beringia (NW North America) – A systematic review of multi-proxy evidence, Quat. Sci. Rev., 147, 312–339, doi:10.1016/j.quascirev.2015.10.021, 2016.
Kennedy, K. E., Froese, D. G., Zazula, G. D. and Lauriol, B.: Last Glacial Maximum age for the northwest Laurentide maximum from the Eagle River spillway and delta complex, northern Yukon, Quat. Sci. Rev., 29(9–10), 1288–1300, doi:10.1016/j.quascirev.2010.02.015, 2010.
Korte, M., Constable, C., Donadini, F. and Holme, R.: Reconstructing the Holocene geomagnetic field, Earth Planet. Sci. Lett., 312(3–4), 497–505, doi:10.1016/j.epsl.2011.10.031, 2011.
Kuehn, S. C., Froese, D. G. and Shane, P. A. R.: The INTAV intercomparison of electron-beam microanalysis

of glass by tephrochronology laboratories: Results and recommendations, Quat. Int., 246(1–2), 19–47, doi:10.1016/j.quaint.2011.08.022, 2011.

Kyle, P. R., Ponomareva, V. V. and Rourke Schluep, R.: Geochemical characterization of marker tephra layers from major Holocene eruptions, Kamchatka Peninsula, Russia, Int. Geol. Rev., 53(9), 1059–1097, doi:10.1080/00206810903442162, 2011.

Lakeman, T. R., Clague, J. J., Menounos, B., Osborn, G. D., Jensen, B. J. L. and Froese, D. G.: Holocene tephras in lake cores from northern British Columbia, Canada, Can. J. Earth Sci., 45(8), 935–947, doi:10.1139/E08-035, 2008.

Lerbekmo, J. F.: The White River Ash: largest Holocene Plinian tephra, Can. J. Earth Sci., 45(6), 693–700, doi:10.1139/E08-023, 2008.

Litton, C. D. and Buck, C. E.: The Bayesian Approach To the Interpretation of Archaeological Data, Archaeometry, 37(1), 1–24, doi:10.1111/j.1475-4754.1995.tb00723.x, 1995.

Lowe, D. J., Pearce, N. J. G., Jorgensen, M. A., Kuehn, S. C., Tryon, C. A. and Hayward, C. L.: Correlating tephras and cryptotephras using glass compositional analyses and numerical and statistical methods: Review and evaluation, Quat. Sci. Rev., 175, 1–44, doi:10.1016/j.quascirev.2017.08.003, 2017.

Lowe, J. J. and Walker, M. J. C.: Radiocarbon Dating the Last Glacial-Interglacial Transition (Ca. 14–9 14 C Ka Bp) in Terrestrial and Marine Records: The Need for New Quality Assurance Protocols, Radiocarbon, 42(1), 53–68, doi:10.1017/s0033822200053054, 2000.

Lund, S., Keigwin, L. and Darby, D.: Character of Holocene paleomagnetic secular variation in the tangent cylinder: Evidence from the Chukchi Sea, Phys. Earth Planet. Inter., 256, 49–58, doi:10.1016/j.pepi.2016.03.005, 2016.

Mackay, H., Hughes, P. D. M., Jensen, B. J. L., Langdon, P. G., Pyne-O'Donnell, S. D. F., Plunkett, G., Froese, D. G., Coulter, S. E. and Gardner, J. E.: A mid to late Holocene cryptotephra framework from eastern North America, Quat. Sci. Rev., 132, 101–113, doi:10.1016/j.quascirev.2015.11.011, 2016.

McAneney, J. and Baillie, M.: Absolute tree-ring dates for the Late Bronze Age eruptions of Aniakchak and Thera in light of a proposed revision of ice-core chronologies, Antiquity, 93(367), 99–112, doi:10.15184/aqy.2018.165, 2019.

Melekestsev, I. V., Felitsyn, S. B. and Kiryanov, V. Y.: The eruption of Opala in A.D. 500 - the largest explosive eruption in Kamchatka in the Christian era., J. Volcanol. Seismol., 13, 21–36, 1992.

Miller, T. P., McGimsey, R. G., Richter, D. H., Riehle, J. R., Nye, G. J., Yount, M. E. and Dumoulin, J. A.: Catalog of the historically active volcanoes of Alaska, U.S. Dept. of the Interior, U.S. Geological Survey., 1998.

Monteath, A. J., van Hardenbroek, M., Davies, L. J., Froese, D. G., Langdon, P. G., Xu, X. and Edwards, M. E.: Chronology and glass chemistry of tephra and cryptotephra horizons from lake sediments in northern Alaska, USA, Quat. Res., 88(02), 169–178, doi:10.1017/qua.2017.38, 2017.

Moore, T. C., Rea, D. K. and Godsey, H.: Regional variation in modern radiocarbon ages and the hard-water effects in Lakes Michigan and Huron, J. Paleolimnol., 20(4), 347–351, doi:10.1023/A:1007920723163, 1998.

Neal, C. A., McGimsey, R. G., Miller, T. P., Riehle, J. R. and Waythomas, C. F.: Preliminary Volcano-Hazard

Assessment for Aniakchak Volcano , Alaska, USGS Open-File Rep., 00–519, 1–35, 2001.
Nelson, R. E., Carter, L. D. and Robinson, S. W.: Anomalous Radiocarbon Ages from a Holocene Detrital Organic Lens in Alaska and their Implications for Radiocarbon Dating and Paleoenvironmental Reconstructions in the Arctic, Quat. Res., 29(1), 66–71, doi:10.1016/0033-5894(88)90072-5, 1988.
Nielsen, C. H. and Sigurdsson, H.: Quantitative methods for electron microprobe analysis of sodium in natural and synthetic glasses., Am. Mineral., 66(5–6), 547–552, 1981.
Nilsson, A., Holme, R., Korte, M., Suttie, N. and Hill, M.: Reconstructing Holocene geomagnetic field variation: new methods, models and implications, Geophys. J. Int., 198(1), 229–248, doi:10.1093/gji/ggu120, 2014.
Ólafsdóttir, S., Geirsdóttir, Á., Miller, G. H., Stoner, J. S. and Channell, J. E. T.: Synchronizing holocene lacustrine and marine sediment records using paleomagnetic secular variation, Geology, 41(5), 535–538, doi:10.1130/G33946.1, 2013.
Oldfield, F., Thompson, R., Crooks, P. R. J., Gedye, S. J., Hall, V. A., Harkness, D. D., Housley, R. a., McCormac, F. G., Newton, A. J., Pilcher, J. R., Renberg, I. and Richardson, N.: Radiocarbon dating of a recent high latitude peat profile: Stor Åmyran, northern Sweden, The Holocene, 7(3), 283–290, doi:10.1177/095968369700700304, 1997.
Olsson, I. U.: Some problems in connection with the evaluation of C 14 dates, Geol. Föreningen i Stock. Förhandlingar, 96(4), 311–320, doi:10.1080/11035897409454285, 1974.
Oswald, W. W., Anderson, P. M., Brown, T. A., Brubaker, L. B., Hu, F. S., Lozhkin, A. V., Tinner, W. and Kaltenrieder, P.: Effects of sample mass and macrofossil type on radiocarbon dating of arctic and boreal lake sediments, The Holocene, 15(5), 758–767, doi:10.1191/0959683605hl849rr, 2005.
Payne, R. J., Blackford, J. and van der Plicht, J.: Using cryptotephras to extend regional tephrochronologies: An example from southeast Alaska and implications for hazard assessment, Quat. Res., 69(1), 42–55, doi:10.1016/j.yqres.2007.10.007, 2008.
Pearce, C., Varhelyi, A., Wastegärd, S., Muschitiello, F., Barrientos, N., O'Regan, M., Cronin, T. M., Gemery, L., Semiletov, I., Backman, J. and Jakobsson, M.: The 3.6ka Aniakchak tephra in the Arctic Ocean: A constraint on the Holocene radiocarbon reservoir age in the Chukchi Sea, Clim. Past, 13(4), 303–316, doi:10.5194/cp-13-303-2017, 2017.
Pearce, N. J. G., Westgate, J. A., Preece, S. J., Eastwood, W. J. and Perkins, W. T.: Identification of Aniakchak (Alaska) tephra in Greenland ice core challenges the 1645 BC date for Minoan eruption of Santorini, Geochemistry, Geophys. Geosystems, 5(3), doi:10.1029/2003GC000672, 2004.
Pilcher, J. R., Hall, V. A. and McCormac, F. G.: Dates of Holocene Icelandic volcanic eruptions from tephra layers in Irish peats, The Holocene, 5(1), 103–110, doi:10.1177/095968369500500111, 1995.
Plunkett, G.: Tephra-linked peat humification records from Irish ombrotrophic bogs question nature of solar forcing at 850 cal. yr BC, J. Quat. Sci., 21(1), 9–16, doi:10.1002/jqs.951, 2006.
Plunkett, G., Coulter, S. E., Ponomareva, V. V., Blaauw, M., Klimaschewski, A. and Hammarlund, D.: Distal tephrochronology in volcanic regions: Challenges and insights from Kamchatkan lake sediments, Glob. Planet.

Change, 134, 26–40, doi:10.1016/j.gloplacha.2015.04.006, 2015.
Ponomareva, V., Portnyagin, M., Pendea, I. F., Zelenin, E., Bourgeois, J., Pinegina, T. and Kozhurin, A.: A full holocene tephrochronology for the Kamchatsky Peninsula region: Applications from Kamchatka to North America, Quat. Sci. Rev., 168, 101–122, doi:10.1016/j.quascirev.2017.04.031, 2017.
Ponomareva, V., Polyak, L., Portnyagin, M., Abbott, P. M., Zelenin, E., Vakhrameeva, P. and Garbe-Schönberg, D.: Holocene tephra from the Chukchi-Alaskan margin, Arctic Ocean: Implications for sediment chronostratigraphy and volcanic history, Quat. Geochronol., 45(November 2017), 85–97, doi:10.1016/j.quageo.2017.11.001, 2018.
Portnyagin, M. V., Ponomareva, V. V., Zelenin, E. A., Bazanova, L. I., Pevzner, M. M., Plechova, A. A., Rogozin, A. N. and Garbe-Schönberg, Di.: TephraKam: Geochemical database of glass compositions in tephra and welded tuffs from the Kamchatka volcanic arc (northwestern Pacific), Earth Syst. Sci. Data, 12(1), 469–486, doi:10.5194/essd-12-469-2020, 2020.
Preece, S. J., McGimsey, R. G., Westgate, J. A., Pearce, N. J. G., Hart, W. K. and Perkins, W. T.: Chemical complexity and source of the White River Ash, Alaska and Yukon, Geosphere, 10(5), 1020–1042, doi:10.1130/GES00953.1, 2014.
Pyne-O'Donnell, S. D. F., Hughes, P. D. M., Froese, D. G., Jensen, B. J. L., Kuehn, S. C., Mallon, G., Amesbury, M. J., Charman, D. J., Daley, T. J., Loader, N. J., Mauquoy, D., Street-Perrott, F. A. and Woodman-Ralph, J.: High-precision ultra-distal Holocene tephrochronology in North America, Quat. Sci. Rev., 52, 6–11, doi:10.1016/j.quascirev.2012.07.024, 2012.
Reuther, J., Potter, B., Coffman, S., Smith, H. and Bigelow, N.: Revisiting the Timing of the Northern Lobe of the White River Ash Volcanic Event in Eastern Alaska and Western Yukon, Radiocarbon, 62(1), 169–188, doi:10.1017/RDC.2019.110, 2020.
Riehle, J. R., Meyer, C. E., Ager, T. A., Kaufman, D. S. and Ackerman, R. E.: The Aniakchak tephra deposit, a Late Holocene marker horizon in western Alaska., 1987.
Schoning, K., Charman, D. J. and Wastegård, S.: Reconstructed water tables from two ombrotrophic mires in eastern central Sweden compared with instrumental meteorological data, The Holocene, 15(1), 111–118, doi:10.1191/0959683605hl772rp, 2005.
Schuur, E. A. G., Bockheim, J., Canadell, J. G., Euskirchen, E., Field, C. B., Goryachkin, S. V., Hagemann, S., Kuhry, P., Lafleur, P. M., Lee, H., Mazhitova, G., Nelson, F. E., Rinke, A., Romanovsky, V. E., Shiklomanov, N., Tarnocai, C., Venevsky, S., Vogel, J. G. and Zimov, S. A.: Vulnerability of Permafrost Carbon to Climate Change: Implications for the Global Carbon Cycle, Bioscience, 58(8), 701–714, doi:10.1641/B580807, 2008.
Steen, D. P., Stoner, J. S., Kaufman, D. S. and Briner, J. P.: 21,000 years of paleomagnetic secular variation and relative paleointensity at Cascade Lake, north-central Brooks Range, Arctic Alaska: Assessing offsets between PSV and radiocarbon-based age models (submitted), Geochronology, n.d.
Stelling, P., Gardner, J. E. and Begét, J.: Eruptive history of Fisher Caldera, Alaska, USA, J. Volcanol. Geotherm. Res., 139(3–4), 163–183, doi:10.1016/j.jvolgeores.2004.08.006, 2005.
Stoner, J. S., Channell, J. E. T., Mazaud, A., Strano, S. E. and Xuan, C.: The influence of high-latitude flux

lobes on the Holocene paleomagnetic record of IODP Site U1305 and the northern North Atlantic, Geochemistry, Geophys. Geosystems, 14(10), 4623–4646, doi:10.1002/ggge.20272, 2013.

Swindles, G. T., De Vleeschouwer, F. and Plunkett, G.: Dating peat profiles using tephra: stratigraphy, geochemistry and chronology, Mires Peat, 7, 1–9, 2010.

Turney, C. S. M., Coope, G. R., Harkness, D. D., Lowe, J. J. and Walker, M. J. C.: Implications for the Dating of Wisconsinan (Weichselian) Late-Glacial Events of Systematic Radiocarbon Age Differences between Terrestrial Plant Macrofossils from a Site in SW Ireland, Quat. Res., 53(1), 114–121, doi:10.1006/qres.1999.2087, 2000.

Tylmann, W., Bonk, A., Goslar, T., Wulf, S. and Grosjean, M.: Calibrating 210Pb dating results with varve chronology and independent chronostratigraphic markers: Problems and implications, Quat. Geochronol., 32, 1–10, doi:10.1016/j.quageo.2015.11.004, 2016.

Vinther, B. M., Clausen, H. B., Johnsen, S. J., Rasmussen, S. O., Andersen, K. K., Buchardt, S. L., Dahl-Jensen, D., Seierstad, I. K., Siggaard-Andersen, M. L., Steffensen, J. P., Svensson, A., Olsen, J. and Heinemeier, J.: A synchronized dating of three Greenland ice cores throughout the Holocene, J. Geophys. Res. Atmos., 111(13), doi:10.1029/2005JD006921, 2006.

Waitt, R. B. and Begét, J. E.: Volcanic processes and geology of augustine volcano, Alaska, US Geol. Surv. Prof. Pap., (1762), 1–78 [online] Available from: http://www.scopus.com/inward/record.url?eid=2-s2.0-80053057972&partnerID=tZOtx3y1, 2009.

Watson, E. J., Swindles, G. T., Lawson, I. T. and Savov, I.: Spatial variability of tephra and carbon accumulation in a Holocene peatland, Quat. Sci. Rev., 124, 248–264, doi:10.1016/j.quascirev.2015.07.025, 2015.

Zander, P. D., Kaufman, D. S., Mckay, N. P., Kuehn, S. C. and Henderson, A. C. G.: Quaternary Geochronology Using correlated tephras to re fi ne radiocarbon-based age models , upper and lower Whitshed Lakes , south-central Alaska, Quat. Geochronol., 45(October 2017), 9–22, doi:10.1016/j.quageo.2018.01.005, 2018.

Zoltai, S. C.: Late Quaternary volcanic ash in the peatlands of central Alberta, Can. J. Earth Sci., 26(2), 207–214, doi:10.1139/e89-017, 1989.

Page 6: [1] Deleted **Lauren Davies** **13/12/2021 10:00:00**

Page 11: [2] Deleted **Lauren Davies** **13/12/2021 10:00:00**

Page 11: [2] Deleted **Lauren Davies** **13/12/2021 10:00:00**

Page 11: [2] Deleted **Lauren Davies** **13/12/2021 10:00:00**

Page 11: [3] Formatted Table **Lauren Davies** **13/12/2021 10:00:00**

Formatted Table

Page 11: [4] Formatted Table **Lauren Davies** **13/12/2021 10:00:00**

Formatted Table

Page 12: [5] Deleted **Lauren Davies** **13/12/2021 10:00:00**

Page 12: [6] Formatted **Lauren Davies** **13/12/2021 10:00:00**

Font: 9 pt, Bold